Temperate Earth-sized planets transiting a nearby ultracool dwarf star

Michaël Gillon[1], Emmanuël Jehin[1], Susan M. Lederer[2], Laetitia Delrez[1], Julien de Wit[3], Artem Burdanov[1], Valérie Van Grootel[1], Adam Burgasser[4,5], Cyrielle Opitom[1], Amaury H. M. J. Triaud[6], Brice-Olivier Demory[6], Devendra K. Sahu[7], Daniella Bardalez Gagliuffi[4,5], Pierre Magain[1] & Didier Queloz[6]

[1]Institut d'Astrophysique et de Géophysique, Université de Liège, Allée du 6 Août 19C, 4000 Liège, Belgium

[2]NASA Johnson Space Center, 2101 NASA Parkway, Houston, Texas, 77058, USA

[3]Department of Earth, Atmospheric and Planetary Sciences, Massachusetts Institute of Technology, 77 Massachusetts Avenue, Cambridge, MA 02139, USA

[4]Center for Astrophysics and Space Science, University of California San Diego, La Jolla, CA, 92093, USA

[5]Visiting Astronomer at the Infrared Telescope Facility, which is operated by the University of Hawaii under Cooperative Agreement no. NNX-08AE38A with the National Aeronautics and Space Administration, Science Mission Directorate, Planetary Astronomy Program

[6]Cavendish Laboratory, J J Thomson Avenue, Cambridge, CB3 0HE, UK

[7]Indian Institute of Astrophysics, Koramangala, Bangalore 560 034, India

Stellar-like objects with effective temperatures of 2700K and below are referred to as "ultracool dwarfs"[1]. This heterogeneous group includes both extremely low-mass stars and brown dwarfs (substellar objects not massive enough to sustain hydrogen fusion), and represents about 15% of the stellar-like objects in the vicinity of the Sun[2]. Based on the small masses and sizes of their protoplanetary disks[3,4], core-accretion theory for ultracool dwarfs predicts a large, but heretofore undetected, population of close-in terrestrial planets[5], ranging from metal-rich Mercury-sized planets[6] to more hospitable volatile-rich Earth-sized planets[7]. Here we report the discovery of three short-period Earth-sized planets transiting an ultracool dwarf star 12 parsecs away. The inner two planets receive four and two times the irradiation of Earth, respectively, placing them close to the inner edge of the habitable zone of the star[8]. Eleven orbits remain possible for the third planet based on our data, the most likely resulting in an irradiation significantly smaller than Earth's. The infrared brightness of the host star combined with its Jupiter-like size offer the possibility of constraining the composition and thoroughly characterizing the atmospheric properties of the components of this nearby planetary system, notably to detect potential biosignatures.

TRAPPIST[9] (TRAnsiting Planets and PlanetesImals Small Telescope) is a robotic 60-cm telescope located at the La Silla European Southern Observatory (ESO) in Chile. Roughly 40% of TRAPPIST's observational time is devoted to the high-cadence photometric monitoring of ~60 southern dwarfs[10] of spectral type later than M5 and with J-magnitude brighter than 12. This program is designed to search for planetary transits and to assess the high-frequency variability of the coolest dwarf stars and very nearby brown dwarfs[11]. This is the prototype of a more ambitious photometric survey called SPECULOOS[12], which will explore the ~500 brightest southern ultracool dwarfs for transiting planets commencing in 2016.

TRAPPIST monitored the brightness of the star TRAPPIST-1 (=2MASS J23062928-0502285) in the very near infrared (~0.9 μm) at high-cadence (~1.2-min) for 245-hours over 62 nights from 17 September to 28 December 2015. The resulting light curves show eleven clear transit-like signatures with amplitudes close to 1% (Extended Data Figs. 1 & 2). Owing to the extensive TRAPPIST dataset and photometric follow-up observations in the visible with the Himalayan Chandra 2m Telescope (India), and in the infrared with the 8m Very Large Telescope (Chile) and the 3.8m UKIRT telescope (Hawaii), nine transits can be attributed to two planets, TRAPPIST-1b and TRAPPIST-1c, transiting the star every 1.51 days and 2.42 days, respectively (Fig. 1 & 2). We attribute the two additional transit signals to a third transiting planet, TRAPPIST-1d, for which 11 orbital periods from 4.5 to 72.8-days are possible based on non-continuous observations (see Table 1). We cannot discard the possibility that the two transits attributed to TRAPPIST-1d originate in fact from two different planets, but the consistency of their main parameters (duration, depth, impact parameter) as derived from their individual analyses does not favour this alternative scenario.

TRAPPIST-1 is a well-characterized, isolated M8.0±0.5-type dwarf star[13] at a distance of 12.0±0.4 parsecs as measured by its trigonometric parallax[14], with an age constrained to be > 500 Myr, and with a luminosity, mass, and radius of 0.05%, 8% and 11.5% those of the Sun[15], respectively. We measured its metallicity to be solar based on the analysis of newly acquired infrared spectra (see Methods). The small size of the host star, only slightly larger than Jupiter, translates into Earth-like radii for the three discovered planets, as deduced from their transit depths. Table 1 presents the physical properties of TRAPPIST-1 and its three planets, as derived through a global Bayesian analysis of the transit photometry (Fig. 1) including the *a priori* knowledge of its stellar properties, with an adaptive Markov-Chain Monte Carlo (MCMC) code[16] (see Methods).

A non-planetary origin of the transit-like signals is fully discarded by several elements. The first element is the high-proper motion of the star (>1"/yr) that allowed confirmation through archival images that no background source of significant brightness was located behind it in 2015 (see Extended Data Fig. 3 and Methods). The second element is the nonexistence of a physical companion of stellar-like nature (star or brown dwarf) around the star, as demonstrated by high-resolution images, radial velocities (RVs), and near-infrared spectroscopy (see Methods). Together, these two first elements demonstrate that the signals do not originate from eclipses of larger bodies in front of either a background or a physically associated stellar-like object blended with the ultracool target star. They also establish that the light of the target is not diluted by an unresolved additional stellar-like object, validating that the measured transit depths result in terrestrial-sized planetary radii. Other elements include the significant age of the star[15], its moderate activity[17] and rotation (vsin=6±2 kms^{-1}; P_{rot} = 1.40±0.05 days as measured from TRAPPIST photometry), and its low level of photometric variability[18] (confirmed by TRAPPIST photometry, see Methods), which are inconsistent with exotic scenarios based on ultra-fast rotation of photospheric structures or occultations by circumstellar material of non-planetary origin (e.g. disk patches, comets)[19].

Further confirmations of the planetary origin of the transits come from (1) the periodicity of the transits of TRAPPIST-1b and TRAPPIST-1c, and the achromaticity of the transits of TRAPPIST-1b as observed from 0.85 μm (HCT) to 2.09 μm (VLT) (Fig. 1); and (2) the

agreement between the stellar density measured from the transit light curves, $49.3^{+4.1}_{-8.3}\,\rho_{\odot}$, with the density inferred from the stellar properties, $55.3\pm12.1\,\rho_{\odot}$ (see Methods).

The masses of the planets and thus their compositions remain unconstrained by these observations. Planetary thermal evolution models and the intense XUV emission of low-mass stars[20] during their early lifes make thick H/He gas envelopes highly unlikely for such small planets[21]. The paucity of material in the inner region of an ultracool dwarf protoplanetary disk[6] favours a composition dominated by ice-rich material originating from beyond the ice line[7]. The confirmation of this hypothesis requires precise mass measurements to be able to break the degeneracy between the relative amounts of iron, silicates, and ice[22]. The semi-amplitudes of the planets' radial velocity (RV) signatures should be between 0.5 and a few ms^{-1}, depending on their compositions. The star is far too faint in the optical (visual magnitude = 18.8)[13] for the measurement of such small signals with existing high-precision optical Doppler instruments. Several high-precision infrared velocimeters designed to reach Doppler precision of 1 $m.s^{-1}$ for infrared-bright stars like TRAPPIST-1 are currently in preparation (e.g. SPIRou[23]). Once in operation, they should bring valuable constraints on the composition of the TRAPPIST-1 planets. Alternatively, the planets' masses could be constrained by the transit timing variations (TTVs) caused by their mutual gravitational interactions[24]. Dynamical simulations assuming Earth-masses for the three planets result in expected TTV amplitudes of the order of a few tens of seconds, within the reach of an intensive campaign of photometric monitoring of the transits at high-cadence and high-precision with world-class telescopes (e.g. VLT & UKIRT, see Extended Data Table 4). The small declination of the star (-5°) makes the follow-up of the system possible from northern and southern ground-based facilities alike.

Given their short orbital distances, it is likely that the TRAPPIST-1 planets are tidally locked, i.e. that their rotations have been synchronized with their orbits by tidal interactions with the host star[25]. Although TRAPPIST-1b and TRAPPIST-1c are not in the host star's habitable zone[8] (HZ, 0.024 to 0.049 astronomical unit, as defined by 1D models that are unfortunately not adequate for modelling the highly asymmetric climate of tidally-locked planets[26]), they have low enough equilibrium temperatures to possibly present habitable regions, in particular, the western terminators of their daysides[26] (see Table 1). The main concern regarding the localized habitability on tidally-locked planets relates to atmospheric and/or water trapping on their night sides[27]. Nevertheless, the relatively large equilibrium temperatures of TRAPPIST-1b and TRAPPIST-1c would likely prevent such trapping[26]. In contrast, TRAPPIST-1d orbits within or beyond the HZ of the star, its most likely periods corresponding to semi-major axes between 0.033 and 0.093 astronomical units (see Methods). Unlike the two inner planets, we estimate tidal circularization timescales for TRAPPIST-1d to be larger than 1 Gyr. Tidal heating due to a non-zero orbital eccentricity could thus have a significant influence on its global energy budget and its potential habitability[28].

The three discovered planets are particularly well-suited for detailed atmospheric characterization by transit transmission spectroscopy (see Fig. 3 and Supplementary Methods), as transit signals are inversely proportional to the square of the host-star radius. Data taken with the *Hubble Space Telescope* (HST) could offer initial constraints on the

extent and composition of their atmospheric terminators. The next generation of observatories should allow for a far more in-depth exploration of their atmospheric properties. In particular, data from the *James Webb Space Telescope* (JWST) should yield strong constraints on the planet masses[29], atmospheric temperatures, and abundances of molecules with large absorption bands, including several biomarkers like H_2O, CO_2, CH_4, and O_3. Complementary insights into the planets' atmospheres should be accessible via the cross-correlation technique[30] applied to high-resolution spectra obtained with the next-generation giant ground-based telescopes (e.g. the European Extremely Large Telescope). Notably, this allows for the detection of both strong absorption lines, which can be opaque at pressures well below 1-Pa (i.e. above a high-altitude cloud deck), as well as weaker absorption bands created by molecules like O_2.

In summary, this discovery provides us with the opportunity to thoroughly characterize a system of three planets similar in size and temperature to Venus and the Earth (Supplementary Fig. 1), opening the young field of comparative exoplanetology to the realm of terrestrial, potentially habitable planets. The detection of this planetary system around one of only the ~60 targets comprising our TRAPPIST survey is suggestive of a high-frequency of close-in Earth-sized planets reaching the bottom of the main sequence and perhaps below (Fig. 4), strengthening the important scientific potential of transit survey projects optimized for the exploration of ultracool dwarfs[12].

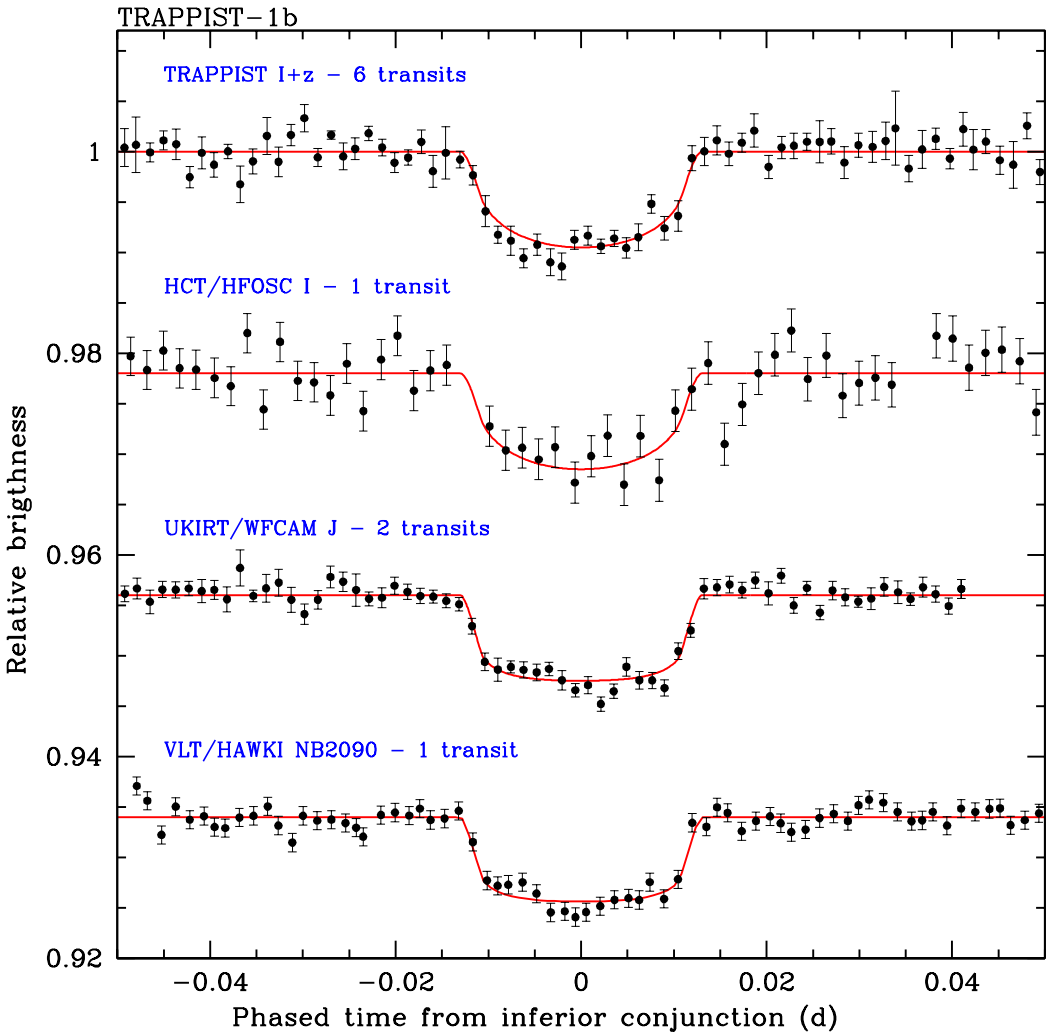

158

159 **Figure 1 | Transit photometry of the planet TRAPPIST-1b**. Each light curve is phased to
160 the time of inferior conjunction (mid-transit time) of the object and binned by 2 minute
161 intervals. The best-fit transit models as derived from the global analysis of the data are
162 overplotted on the light curves (red lines). The light curves are shifted along the *y*-axis for the
163 sake of clarity. For the HCT/HFOSC light curve, each bin includes only one measurement
164 and the error bars are the formal measurement errors. For the other light curves, the error bars
165 are the standard errors of the mean of the measurements in the bin.

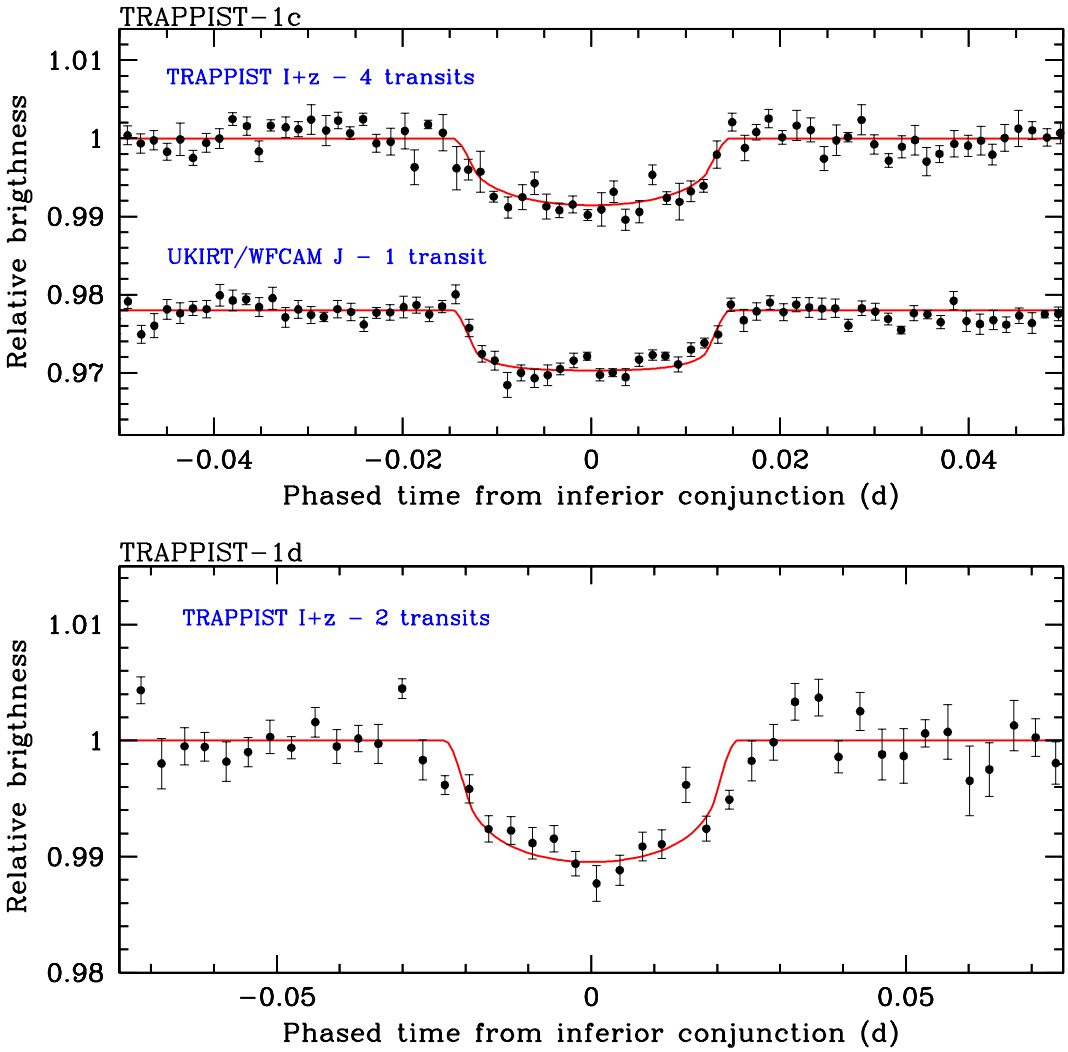

166

167 **Figure 2 | Transit photometry of the planet TRAPPIST-1c and TRAPPIST-1d**. Same as
168 Fig. 1, except that the light curve of TRAPPIST-1d is binned per 5 minute intervals for the
169 sake of clarity. The error bars are the standard errors of the mean of the measurements in the
170 bin.

171

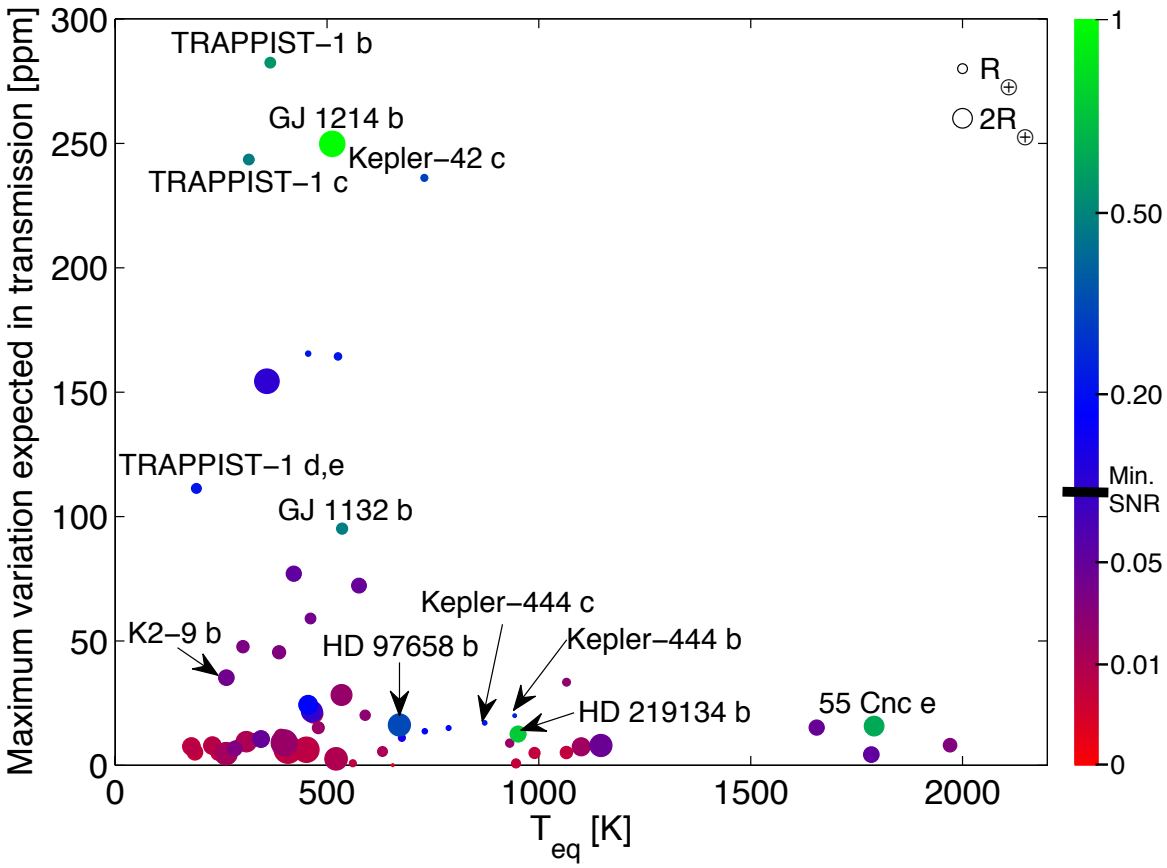

Figure 3 | Comparison of the known sub-Neptune-size exoplanets in terms of temperature and suitability for detailed atmospheric characterization. Estimation of the signal (in ppm, parts per million) and signal-to-noise ratio (SNR) in transmission (normalized to the SNR for GJ1214b) versus equilibrium temperatures (T_{eq}) assuming a null Bond albedo. Only the exoplanets with a measured radius smaller than 3 Earth radii are included in the figure. "Min. SNR" indicates the minimum SNR required for the atmospheric characterization of a target with JWST over its lifetime. The size of the circular symbol of each planet is proportional to its physical size.

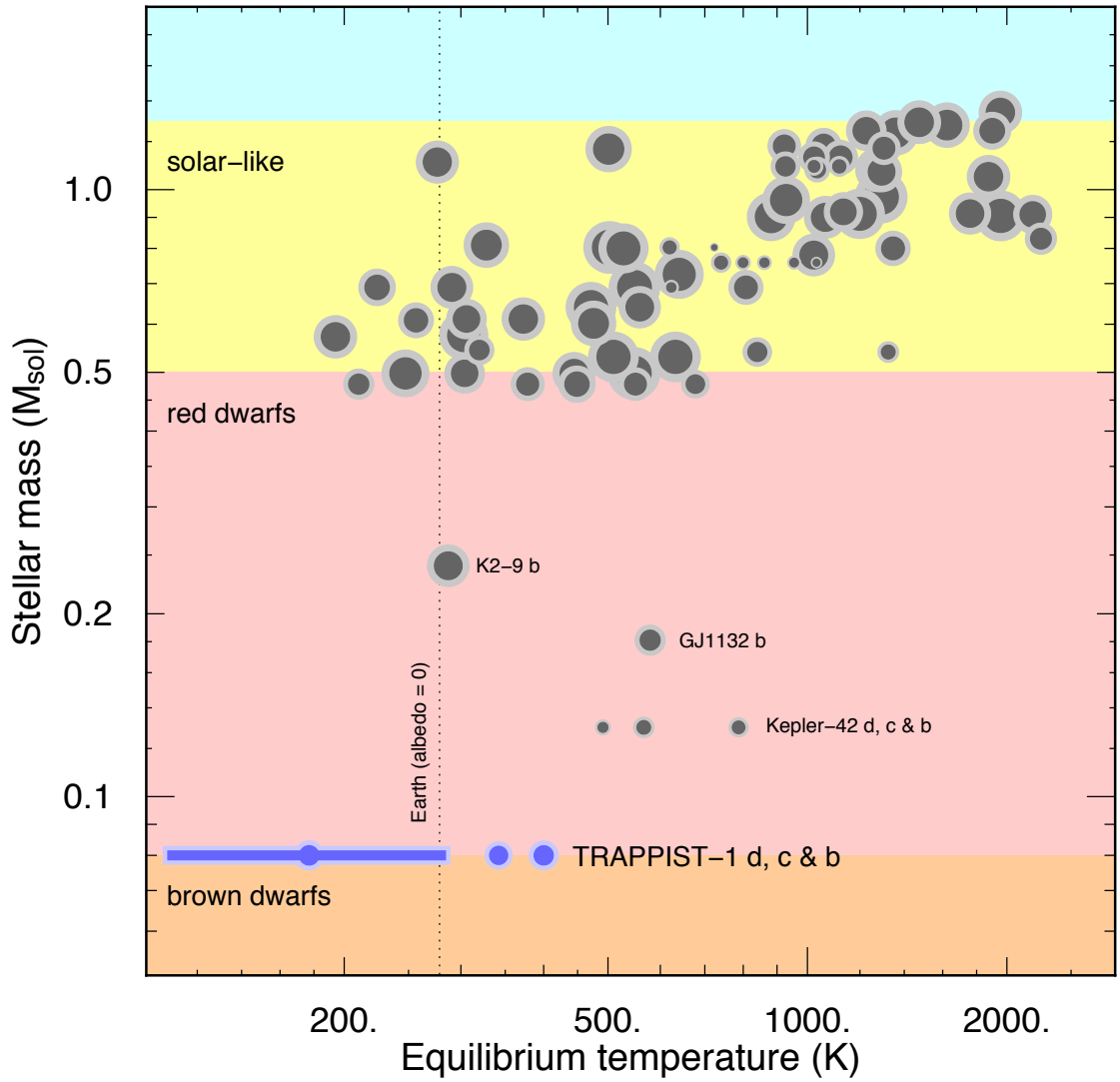

Figure 4 | Comparison of the known sub-Neptune-size exoplanets in terms of temperature and mass of the host star. The size of the symbols linearly scales with planet radius. The background is color-coded as a function of stellar mass (in units of the Sun's mass). TRAPPIST-1 is at the boundary between hydrogen burning stars and brown dwarfs. Equilibrium temperatures are estimated neglecting atmospheric effects and assuming an albedo of 0. The position of the Earth is given with a dotted line, for reference. The range of possible equilibrium temperatures of TRAPPIST-1d is represented by a solid bar. The location of the dot is the most likely solution.

Table 1 | Properties of the TRAPPIST-1 planetary system

Parameter	Value		
Star	**TRAPPIST-1 = 2MASS J23062928-0502285**		
Magnitudes	V=18.80±0.08, R=16.47±0.07, I=14.0±0.1, J=11.35±0.02, K=10.30±0.02		
Distance $d_\star$	12.1±0.4 parsecs[14]		
Luminosity $L_\star$	0.000525±0.000036 $L_\odot$[15]		
Mass $M_\star$	0.080±0.009 $M_\odot$		
Radius $R_\star$	0.114±0.006 $R_\odot$		
Density $\rho_\star$	$50.3^{+5.7}_{-3.3}$ $\rho_\odot$		
Effective temperature T_{eff}	2550±55 K		
Metallicity [Fe/H]	+0.04±0.08 (from near-IR spectra, see Methods)		
Rotation period P_{rot}	1.40±0.05d (from TRAPPIST photometry, see Methods)		
Age $\tau_\star$	>500 Myr[15]		
Planets	**TRAPPIST-1b**	**TRAPPIST-1c**	**TRAPPIST-1d**
Orbital period P	1.510848 ±0.000019d	2.421848 ±0.000028d	{4.551, 5.200, 8.090, 9.101, 10.401, 12.135, 14.561, **18.202**, 24.270, 36.408, 72.820}d[a]
Mid-transit time t_0 - 2,450,000 [BJD_{TDB}]	7322.51765 ±0.00025	7362.80520 ±0.00033	7294.7744 ±0.0015[b]
Transit depth $(R_p/R_\star)^2$	0.754±0.025 %	0.672±0.042 %	0.826±0.073%[b]
Transit impact parameter b	0.21±0.14 $R_\star$	0.25±0.15 $R_\star$	0.20±0.15 $R_\star$[b]
Transit duration W	36.12±0.46 min	41.78±0.81 min	83.3±2.5 min[b]
Orbital inclination i	89.41±0.41 deg	89.50±0.31 deg	89.90±0.10 deg[b]
Orbital eccentricity e	0 (fixed)	0 (fixed)	0 (fixed)
Radius R_p	1.113±0.044 R_{Earth}	1.049±0.050 R_{Earth}	1.163±0.065 R_{Earth}[b]
Scale parameter $a/R_\star$	$20.45^{+0.43}_{-0.81}$	$28.0^{+0.6}_{-1.1}$	{41:271}[c]
Semi-major axis a	0.01111 ±000040 au	0.01522 ±0.00055 au	{0.022:0.146}[c] au
Irradiation S_p	4.25±0.38 S_{Earth}	2.26±0.21 S_{Earth}	{0.02:1.0}[c] S_{Earth}
Equilibrium temperature T_{eq}			
with Bond albedo of 0.00	400±9 K	342±8 K	{110:280}[c] K
with Bond albedo of 0.75	285±7 K	242±6 K	{75:200}[c] K

The values and 1-sigma errors given for the planetary parameters and for the stellar mass, radius, density, and effective temperature were deduced from a global analysis of the photometric data, including *a priori* knowledge on the stellar properties (see Methods).

[a]These are the potential orbital periods of TRAPPIST-1d based on non-continuous observations.

[b]Assuming P=18.20175±0.00045d , the most likely values for the period as derived from the shape of the transits.

[c]Range allowed by the set of possible periods.

Supplementary information is available in the online version of the paper.

Acknowledgments. TRAPPIST is a project funded by the Belgian Fund for Scientific Research (F.R.S.-FNRS) under grant FRFC 2.5.594.09.F, with the participation of the Swiss National Science Foundation. The material presented here is based on work supported in part by the National Aeronautics and Space Administration under Contract No. NNX15AI75G. The VLT/HAWK-I data used in this work were obtained in the Director Discretionary Time (DDT) program 296.C-5010. M. Gillon, E. Jehin, and V. Van Grootel are F.R.S.-FNRS Research Associates. L. Delrez acknowledges support of the F.R.I.A. fund of the F.R.S-FNRS. The authors thank the Liverpool Telescope team, Ö. Baştürk, and M. Bretton for their attempts to measure the transits of the TRAPPIST-1 planets from La Palma, Turkey, and France, respectively; the IRTF operators B. Cabreira and D. Griep for their assistance with the SpeX observations; the UKIRT staff scientists W. Varricatt & T. Kerr, telescope operators S. Benigni, E. Moore, and T. Carroll, and CASU scientists G. Madsen and M. Irwin for their assistance with the UKIRT observations; the ESO astronomers A. Smette & G. Hau for their diligent efforts to provide us with the best possible VLT data; the staff of IAO, Hanle and CREST, Hosakote, that made observations with HCT possible. The facilites at IAO and CREST are operated by the Indian Institute of Astrophysics, Bangalore, India.

Author Contributions. The TRAPPIST team (MG, EJ, LD, ArB, CO, PM) managed the TRAPPIST observations, discovered the planets, organized the follow-up observations, and led the analysis and interpretation. MG leads the exoplanet program of TRAPPIST, set up and organized the ultracool dwarf transit survey, planned and analysed a part of the TRAPPIST, UKIRT, and VLT observations, and led their scientific exploitation. EJ manages the maintenance and the operations of the TRAPPIST telescope. SL obtained the DDT time on UKIRT, managed with EJ the preparation of the UKIRT observations, and assisted in writing the manuscript. LD and CO scheduled and performed some of the TRAPPIST observations. LD and ArB analysed some of the TRAPPIST and UKIRT photometric observations. ArB assessed the possible existence of a background object blended with the star. JdW took in charge the study of the amenability of the planets for detailed atmospheric characterization and assisted MG for the habitability discussion. BOD took charge of the dynamical simulations. AdB checked the spectral type of the star and determined its metallicity. DBG acquired the SpeX spectra. DS gathered the HCT observations. VVG checked physical parameters of the star and performed stellar evolutionary modelling. PM is the administrative manager of TRAPPIST. AT, PM and DQ assisted in analysis and writing the manuscript.

Author Information. Reprints and permissions information is available at www.nature.com/reprints. The authors declare no competing financial interests. Readers are welcome to comment on the online version of the paper. Correspondence and requests for materials should be addressed to M.G. (michael.gillon@ulg.ac.be).

Online Content. Methods, along with any additional Extended Data display items and Source Data, are available in the online version of the paper; references unique to these sections appear only in the online paper.

METHODS

Spectral type, parallax, and age of the star.

TRAPPIST-1 = 2MASS J23062928-0502285 was discovered in 2000 by a search for nearby ultracool dwarfs based on photometric criteria[31] and identified as a high proper-motion (μ_α=0.89", μ_δ=-0.42"), moderately active ($\log L_{H\alpha}/L_{bol}$=-4.61), M7.5 dwarf at ~11 parsecs. Subsequent studies converged to a spectral type of M8.0±0.5[13, 32], while confirming a moderate level of activity typical of similar spectral type stars in the vicinity of the Sun[16, 33, 34]. We checked this spectral classification by comparing a low-resolution (R~150) near-infrared spectrum of the star[15] obtained with the SpeX spectrograph[35] mounted on the 3m NASA Infrared Telescope Facility to several spectral type standards, and obtained the best-fit with the spectrum of the M8-type standard LHS 132 (Extended Data Fig. 4). The CTIOPI project measured the star's trigonometric parallax to be π=82.6±2.6 mas[14], translating into a distance of 12.1±0.4 parsecs. High-resolution optical spectroscopy failed to detect significant absorption at the 6708 Å Li line[36], inferring that the object is not a very young brown dwarf but rather a very-low-mass main-sequence star. This is in agreement with its thick disk kinematics[36], its relatively slow rotation (vsini=6±2 km.s^{-1})[16], its moderate activity, and its reported photometric stability[17] that all point to an age of at least 500 Myrs[15].

Metallicity of the star.

We obtained new near-infrared (0.9-2.5 μm) spectroscopy of TRAPPIST-1 with the SpeX spectrograph on the night of 2015 November 18 (UT) during clear conditions and 0.8" seeing at K-band. We used the cross-dispersed mode and 0.3"x15" slit aligned at the parallactic angle, to acquire moderate-resolution data ($\lambda/\Delta\lambda \approx 2000$) with dispersion 3.6 Å pixel^{-1} covering the spectral range 0.9-2.5 μm in seven orders. Ten exposures of 300s each were obtained over an airmass range of 1.14-1.17, followed by observations of the A0V star 67 Aqr (V = 6.41) at an airmass of 1.19 for telluric and flux calibration, as well as internal lamp exposures. Data were reduced using the SpeXtool package version 4.04[37, 38] which included optimal extraction, averaging and merging of spectral orders, removal of bad pixels and instrumental effects, wavelength calibration, and correction of slit and atmospheric transmission losses. The reduced spectrum has a median signal-to-noise of 300 in the 2.17-2.35 μm region, which is shown in Extended Data Fig. 5, with metallicity-sensitive NaI (2.206, 2.209 μm) and CaI (2.261, 2.263, 2.266 μm) atomic features labeled. We measured equivalent widths of these features and the H_2O-K2 index defined in Rojas-Ayala et al. (2012)[39], and used the mid- and late-M dwarf metallicity calibration of Mann et al. (2014)[40] to determine [Fe/H] = 0.04±0.02 (measurement) ±0.07 (systematic) for TRAPPIST-1. The quadratic sum of the two errors resulted in our final measurement [Fe/H] = 0.04±0.08.

Basic parameters of the star.

A recent study[15] derived a luminosity $L_\star$ = 0.000525±0.000036 $L_\odot$ for TRAPPIST-1, using as input data the trigonometric parallax and VRI magnitudes as measured by the CTIOPI project[14], 2MASS JHK magnitudes[41], WISE W123 magnitudes[42], an optical spectrum measured with KPNO/R-C Spec[43], and a near-IR spectrum measured by SpeX/Prism. Using this luminosity and the constraint on the age to be >500 Myr as input, the authors of the study[15] derived from evolutionary model isochrones and the Stefan-Boltzmann law the

following values for the stellar mass, radius, and effective temperature: $M_\star$ = 0.082±0.009 $M_\odot$, $R_\star$ = 0.116±0.004 $R_\odot$, and T_{eff} = 2557±64K, respectively. To account for the uncertainties coming from the assumptions and details of the evolutionary models, we performed a new determination of these three basic parameters with the new solar metallicity evolutionary model isochrones of Baraffe et al. (2015)[44] that consistently couple atmosphere and interior structures. We obtained $M_\star$ = 0.089 $M_\odot$, $R_\star$ = 0.112 $R_\odot$, and T_{eff} = 2615K. We then added the difference between the two determinations quadratically to the errors of Filippazzo et al.[15], adopting finally $M_\star$ = 0.082±0.011 $M_\odot$, $R_\star$ = 0.116±0.006 $R_\odot$, and T_{eff} = 2555±85K. The normal distributions corresponding to these values and errors were assumed as prior probability distribution functions in the Bayesian analysis of our photometric data (see below).

Possible binarity of the star.

High-resolution imaging from the ground[45, 46, 47] and from space with HST[48] discarded the existence of a companion down to an angular distance of 0.1", corresponding to a projected physical distance of 1.2 au at 12 parsecs, in good agreement with the reported stability of the radial velocity of the star at the ~10 ms^{-1} level over a week[49] and at the ~150 ms^{-1} level over ~10 weeks[50]. We performed spectral binary template fitting[51] to the IRTF/SpeX spectroscopy, and statistically reject the presence of an L- or T-type brown dwarf companion that would be visible in a blended-light spectrum. TRAPPIST-1 can thus be considered in all probability as an isolated star.

Upper magnitude limits on a background eclipsing binary (BEB).

We measured the J2000 equatorial coordinates of TRAPPIST-1 in the 2015 TRAPPIST images, using 29 stars from the UCAC2 catalog[52] and the Pulkovo Observatory Izmccd astrometric software[53]. We obtained coordinates of RA=23h06m30.34s, DEC=-05d02m36.44s. Due to the high proper motion of TRAPPIST-1 of ~1"/yr, the presence of a possible background object could be assessed by examining this exact position in several previous images taken from the POSS[54] (1953) and 2MASS[41] (1998) image catalogs. No possible additional source was detected at its position in any of these images (Extended Data Fig. 3). The faintest stars detected at other positions in the 2MASS images have J-band magnitudes of ~17. We adopt this value as an absolute lower threshold for the J-band magnitude of a background source blended with TRAPPIST-1 in our TRAPPIST 2015 images. TRAPPIST-1 has a J-band magnitude of 11.35[42], and the achromaticity of the transits of TRAPPIST-1b as observed from 0.85 to 2.09 μm imposes that, if they originated from a BEB, the latter would have to be a very red object with a spectral type similar to TRAPPIST-1. Combining these two facts, the BEB scenario would require an unphysical eclipse depth >100% in the photometric bands probed by our observations to match the ~0.8% depths measured after dilution by the light of TRAPPIST-1. The BEB scenario is thus firmly discarded.

Photometric observations and analysis.

The TRAPPIST[9, 55] observations in which the transits were detected consisted of 12,295 exposures of 55-s gathered with a thermoelectrically-cooled 2kx2k CCD camera (field of view of 22' x 22', pixel scale of 0.65"). Most of the observations were obtained through an

'I+z' filter having a transmittance >90% from 750 nm to beyond 1100 nm, the red end of the effective bandpass as defined by the spectral response of the CCD. Basing on the spectral efficiency model for TRAPPIST and an optical spectrum of a spectroscopic standard M8V star (VB10), we compute an effective wavelength of 885±5 nm for these observations. For the nights of 20 November and 19 December 2015, the target was close to the full Moon and the observations were performed in the Sloan z' filter to minimize the background. The positions of the stars on the chip were kept within a box of a few pixels on a side to improve the photometric precision through instant astrometric calibration of the science images and real-time pointing corrections.

After a standard pre-reduction (bias, dark, flat-field correction), the TRAPPIST automatic pipeline extracted the stellar fluxes from the images using the DAOPHOT aperture photometry software[56] for eight different apertures. A careful selection of both the photometric aperture size and of stable comparison stars was then manually performed to obtain the most accurate differential light curves of TRAPPIST-1. TRAPPIST is equipped with a German equatorial mount, thus the CCD must rotate 180° relative to the stars at the meridian, resulting in different positions of the stellar images before and after the meridian flip. For this reason, the images corresponding to either side of the meridian are reduced separately for each night, resulting in two light curves.

Photometric follow-up observations were performed with the HAWK-I near-IR imager[57] on the ESO 8m Very Large Telescope (Chile), with the HFOSC optical spectro-imager[58] on the 2m *Himalayan Chandra Telescope* (India), and with the WFCAM Wide-Field infrared CAMera[59] located at the prime focus of the 3.8m UKIRT telescope (Hawaii).

The VLT/HAWK-I observations of a transit of TRAPPIST-1b were performed during the night of 8 November 2015. HAWK-I is composed of four Hawaii 2RG 2048 x 2048 pixels detectors (pixel scale = 0.106"). Its total field of view on the sky is 7.5'x7.5'. The transit was observed through the narrowband filter NB2090 (λ=2.095µm, width=0.020µm). 185 exposures composed of 17 integrations of 1.7s each were acquired during the run in stare mode, i.e. without applying a jitter pattern. Pointing was carefully selected by the ESO staff astronomer to avoid cosmetic defects at the locations of TRAPPIST-1 or the potential comparison stars. The calibration of the images and the photometric extraction were performed as described in Gillon et al. (2012)[16].

The HCT/HFOSC observations of a transit of TRAPPIST-1b were performed on 18 November 2015. The imager in the HFOSC CCD detector is an array of 2048x2048 pixels corresponding to a field of view of 10'x10' on-sky (pixel scale=0.3"). The observations consisted of 104 exposures, each 20-s taken in stare mode and in the I filter, centered on the expected transit time. After a standard calibration of these images and their photometric reduction with DAOPHOT, differential photometry was performed. We estimate the effective wavelength of these observations to be 840±20 nm, based on the spectral response of HFOSC and an optical spectrum of the M8V standard star VB10.

The UKIRT/WFCAM observations of 2 transits of TRAPPIST-1b and 1 transit of TRAPPIST-1c consisted of 3 runs of 4 hrs each, performed on 5, 6 and 8 December 2015 in

J-band. WFCAM is composed of four HgCdTe detectors of 2048x2048 pixels each, with a pixel scale of 0.4" resulting in a field of view of 13.65'x13.65' for each detector. On 5 December 2015, 1365 exposures composed of 3 integrations of 2s each were performed in stare mode. Pointing was carefully selected to put TRAPPIST-1 and several comparison stars of similar brightness on the cleanest of the four WFCAM arrays. For the runs on 6 and 8 December 2015, respectively, 1181 and 1142 exposures composed of five 1s-exposures were performed, again in stare mode and using the same pointing as 5 Dec 2015. Differential aperture photometry was performed with DAOPHOT on all calibrated images.

Global analysis of the photometry.

We inferred the parameters of the three detected planets transiting TRAPPIST-1 from the analysis of their transit light curves (Extended Data Fig. 1) with an adaptive Markov-Chain Monte Carlo (MCMC) code[16]. We converted each UT time of mid-exposure to the BJD_{TDB} time system[60]. The model assumed for each light curve was composed of the eclipse model of Mandel & Agol (2002)[61] multiplied by a baseline model aiming to represent the other astrophysical and instrumental mechanisms able to produce photometric variations. Assuming the same baseline model for all light curves, and minimizing the Bayesian Information Criterion (BIC)[62], we selected a second-order time polynomial as a baseline model to represent the curvature of the light curves due to the differential extinction and the low-frequency variability of the star, and added an instrumental model composed of a second-order polynomial function of the positions and widths of the stellar images.

Stellar metallicity, effective temperature, mass, and radius were four free parameters in the MCMC for which prior probability distribution functions (PDFs) were selected as input. Here, the normal distributions $N(0.04, 0.08^2)$ dex, $N(2555, 85^2)$ K, $N(0.082, 0.011^2)$ $M_\odot$, and $N(0.114, 0.006^2)$ $R_\odot$ were assumed based on *a priori* knowledge of the stellar properties (see Basic parameters of the Star). Circular orbits were assumed for all transiting objects. For each of them, the additional free parameters in the MCMC included (1) the transit depth dF defined as $(R_p/R_\star)^2$, with R_p and $R_\star$ the planetary and stellar radii, respectively (2) the transit impact parameter $b = a \cos i/R_\star$, with a and i the planet's semi-major axis and orbital inclination, respectively (3) the orbital period P, (4) the transit width W defined as $(P R_\star/a) [(1+R_p/R_\star)^2 - b^2]^{1/2}/\pi$, and (5) the mid-transit time (time of inferior conjunction) T_0. Uniform prior distributions were assumed for each of these free parameters. At each step of the MCMC, values for R_p, a, i, were computed from the values for the transit and stellar parameters, as well as values for the irradiation of the planet in Earth units and for its equilibrium temperatures assuming a Bond albedo of 0 and 0.75, respectively. A quadratic limb-darkening law[62] was assumed for the star. For each bandpass, values and errors for the limb-darkening coefficients u_1 and u_2 were derived from the Claret & Bloemen tables (2011)[63] (see Extended Data Table 2), and the corresponding normal distributions were used as prior PDFs in the MCMC. u_1 and u_2 were free parameters under the control of these PDFs in the MCMC.

We divided our analysis into two phases. The first phase focused on the two inner planets TRAPPIST-1b and TRAPPIST-1c, for which the period is firmly determined. A circular orbit was assumed for both planets. All transit light curves of the two planets were used as input data for this first phase, except the TRAPPIST light curve of 11 December 2015 for which

the transit of TRAPPIST-1c is blended with a transit of TRAPPIST-1d. A preliminary MCMC analysis composed of 1 chain of 50,000 steps was first performed to estimate the need to rescale the photometric errors as described in Gillon et al. (2012)[16]. Then a longer MCMC analysis was performed, composed of 5 chains of 100,000 steps whose convergence was checked using the statistical test of Gelman & Rubin[64]. The parameters derived from this analysis for the star and its two inner planets are shown in Table 1. We performed a similar analysis assuming a uniform prior PDF for the stellar radius to derive the value of the stellar density constrained only by the transit photometry[65]. It resulted in a stellar density of $49.3^{+4.1}_{-8.3}\,\rho_{\odot}$, in excellent agreement with the density of 55.3±12.1 $\rho_{\odot}$ derived from the *a priori* knowledge of the star, bringing thus a further validation of the planetary origin of the transit signals.

In the second phase of our analysis, we performed 11 global MCMC analyses of all transit light curves, each of them consisting of one chain of 50,000 steps and corresponding to one of the possible values of the period of TRAPPIST-1d (see Table 1) for which a circular orbit was assumed. We then repeated the 11 analyses under the assumption of an eccentric orbit for planet d. We used the medians of the BIC posterior distributions to compare the relative posterior probability of each orbital model for TRAPPIST-1d through the formula $P1/P2 = e^{(BIC_2 - BIC_1)/2}$. The resulting relative probabilities are shown in Extended Data Table 3. It shows that our data favour (relative probability > 10%) a circular orbit and an orbital period between 10.4 and 36.4 days, the most likely period being 18.4 days.

In the final phase, we performed individual analyses of the light curves to measure the mid-eclipse time of each transit to support future TTV studies of the system[24, 66]. The resulting timings are shown in Extended Data Table 4. They do not reveal any significant TTV signal, which is not surprising given the amplitude of the expected TTV signals (see below) combined with the limited timing precision of the TRAPPIST photometry.

Extended Data Fig. 1 and 2 show the raw and detrended light curves, respectively, and for each of these the best-fit eclipse + baseline model is overplotted in the figures. The phased-time detrended light curves are shown for each planet and bandpass in Fig. 1.

Photometric variability of the star.

The TRAPPIST dataset was used to assess the photometric variability of the star at ~900 nm. On the timescale of a few hours, corresponding to the typical duration of our observing runs, the star appears to be relatively stable, except for the transits and for 4 sharp, low-amplitude (1 to a few %), increases of brightness followed by exponential-type decreases to the normal levels within 10-15 minutes (Extended Data Fig. 6) that we attribute to flares[67]. The low amplitude and inferred low frequency (1/60 hr^{-1}) of these flares is consistent with the reported low level of activity of the star[17,33,34], strengthening the inference that the system is not young.

To assess the lower-frequency variability of TRAPPIST-1, we built its global differential light curve in the I+z filter, using four quiet stars of similar brightness in the TRAPPIST images as comparison stars. We filtered out the flares, transits, and measurements taken in cloudy conditions to create the resulting light curve consisting of 12,081 photometric

measurements. It is compared to the light curve for the comparison star 2MASSJ23063445-0507511 in Extended Data Fig. 7. It clearly shows some variability at the few % level, which is consistent with previous photometric results obtained in the I-band[17]. A Lomb-Scargle (LS) periodogram[68] analysis of the light curve, filtered out of low-frequency variations and differential extinction by division of the best-fit 4th-order polynomial in time and airmass, reveals a power excess with a period of 1.4 days. Cutting the light curves in two, and in four in a second test, and performing a LS analysis of each fraction, revealed a power excess at ~1.4 days for all of them, supporting a genuine periodic signal of astrophysical origin. Associating it with the stellar rotation period, the resulting equatorial rotation speed of 4.1 km.s^{-1} (assuming $R_\star$ = 0.114 $R_\odot$) is consistent with the literature measurement[16] vsini=6±2 km.s^{-1}, making this association physically meaningful. Based on the scatter of the peak values obtained in the LS analyses of the light curve fractions, we estimate the error bar on the rotation period of 1.40 days to be 0.05 day. In summary, the photometric variability of the star appears thus to be dominated by the rotation and evolution of photospheric inhomogeneities (spots) combined with rare flares.

Dynamics of the system.

We computed the tidal circularization timescales[69] $t_{circ} = \frac{2PQ}{63\pi} \times \frac{M_p}{M_*} \times \left(\frac{a}{R_p}\right)^5$ of the three planets, assuming planetary masses M_p ranging from 0.45 Earth masses (pure ice composition) to 3 Earth masses (pure iron composition)[21] and a tidal quality factor[70] Q of 100, corresponding to the maximum value derived for terrestrial planets and satellites of the solar system[70]. For TRAPPIST-1b and TRAPPIST-1c, the computed values range from 22 Myr to 145 Myr and from 177 Myr to 1.1 Gyr, respectively. Taking into account that the system is apparently not very young and that the orbits have weak mutual perturbations as they are not close to any mean-motion resonance, our assumption of circular orbits for the two inner planets is thus reasonable. On the other hand, the same computations result in values ranging from a few to tens of Gyr for TRAPPIST-1d, making a significant orbital eccentricity possible from a tidal theory perspective. Still, a nearly-circular orbit for this outer planet is still a reasonable hypothesis when considering the strong anticorrelation of orbital eccentricity and multiplicity of planets detected by radial velocities[71], and is favoured by our global analysis of the transit photometry (see above).

We used the Mercury software package[72] to assess the dynamical stability of the system over 10,000 years for all possible periods of TRAPPIST-1d. Instabilities appeared in our simulations only for the unlikely scenarios of TRAPPIST-1d on a significantly eccentric (e≥0.4) 4.5 or 5.2 day orbit.

To assess the potential of the TTV method[24, 66] to measure the masses of the planets, we integrated the dynamical evolution of the system at high sampling over 2 years, assuming Earth-masses for the three planets and an 18.4 day circular orbit for TRAPPIST-1d. These simulations resulted in TTV amplitudes of several tens of seconds and led us to conclude that with an intensive transit monitoring campaign with instruments able to reach timing

513 precisions of a few tens of seconds (e.g. VLT/HAWK-I, UKIRT/WFCAM, see Extended
514 Table 4), it should be possible to constrain the planetary masses.
515

Code availability. Equivalent widths and H_2O-K2 index measurements in the SpeX spectra were made using the IDL program created by A. Mann and distributed at http://github.com/awmann/metal. The conversion of the UT times of the photometric measurements to the BJD_{TDB} system was performed using the online program created by J. Eastman and distributed at http://astroutils.astronomy.ohio-state.edu/time/utc2bjd.html. IRAF is distributed by the National Optical Astronomy Observatory, which is operated by the Association of Universities for Research in Astronomy, Inc., under cooperative agreement with the National Science Foundation. The MCMC software used to analyse the photometric data is a custom Fortran 90 code that can be obtained upon request to the first author.

Web summary. An ultracool Jupiter-sized star 12 parsecs (36 light-years) away is shown to be periodically eclipsed by three temperate Earth-sized planets with irradiation levels similar to Venus and Earth. All three planets are well-suited for detailed atmospheric characterization, including biosignature detections, with next-generation observatories.

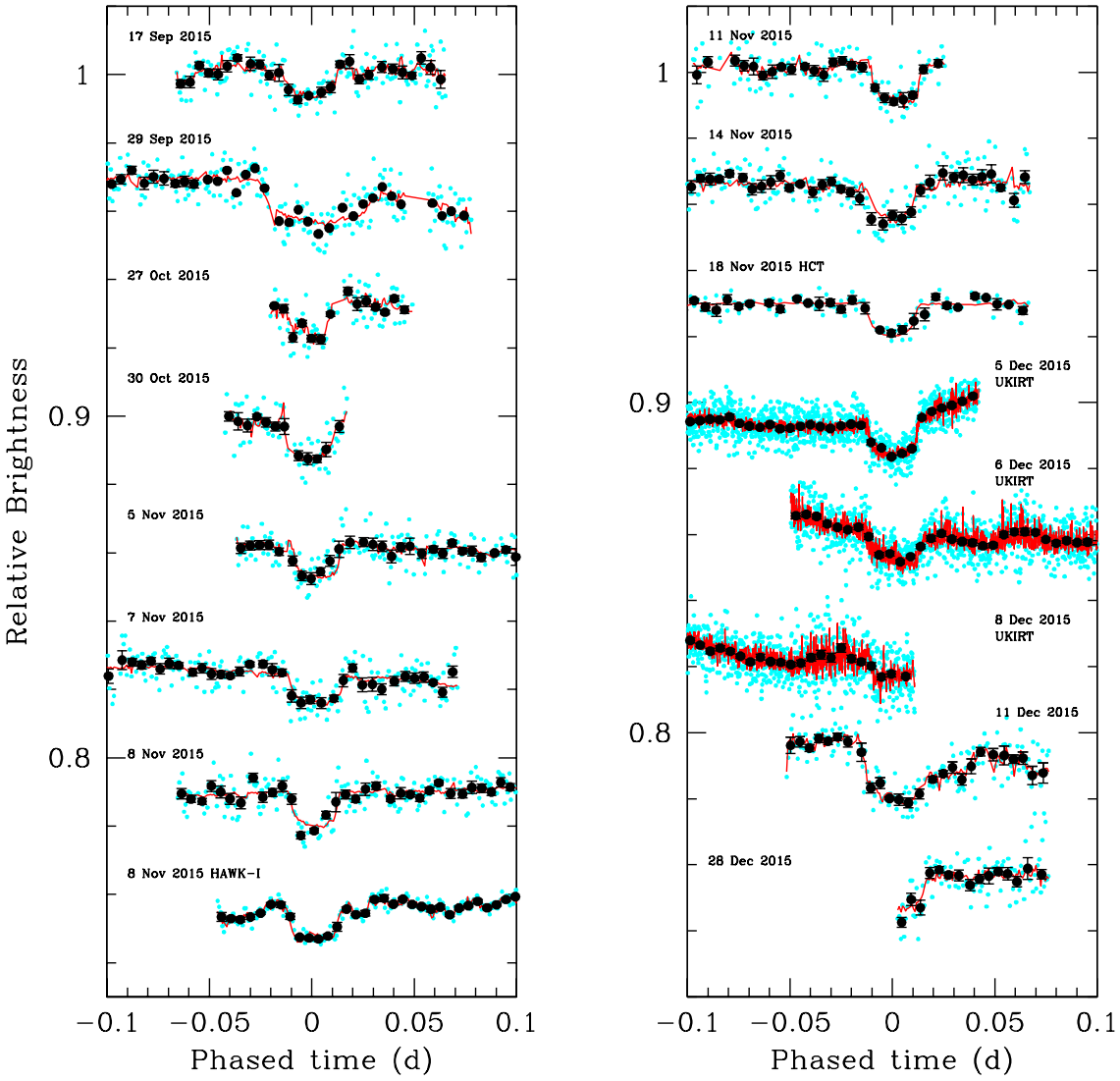

Extended Data Figure 1 | Raw TRAPPIST-1 transit light curves. The light curves are shown in chronological order from top to bottom and left to right, with unbinned (cyan dots) and binned per 0.005-d (7.2-min) intervals (black dots with error bars). The error bars are the standard errors of the mean of the measurements in the bins. The best-fit transit+baseline models are overplotted (red line). The light curves are phased for the mid-transit time and shifted along the *y*-axis for the sake of clarity. For the dual transit of 11 Dec 2015, the light curve is phased for the mid-transit time of TRAPPIST-1c. The UKIRT data were sampled at a much higher frequency (~10x higher) than all other datasets (see Extended Data Table 1). The name of the telescope having acquired the data is given for light curves not obtained by TRAPPIST.

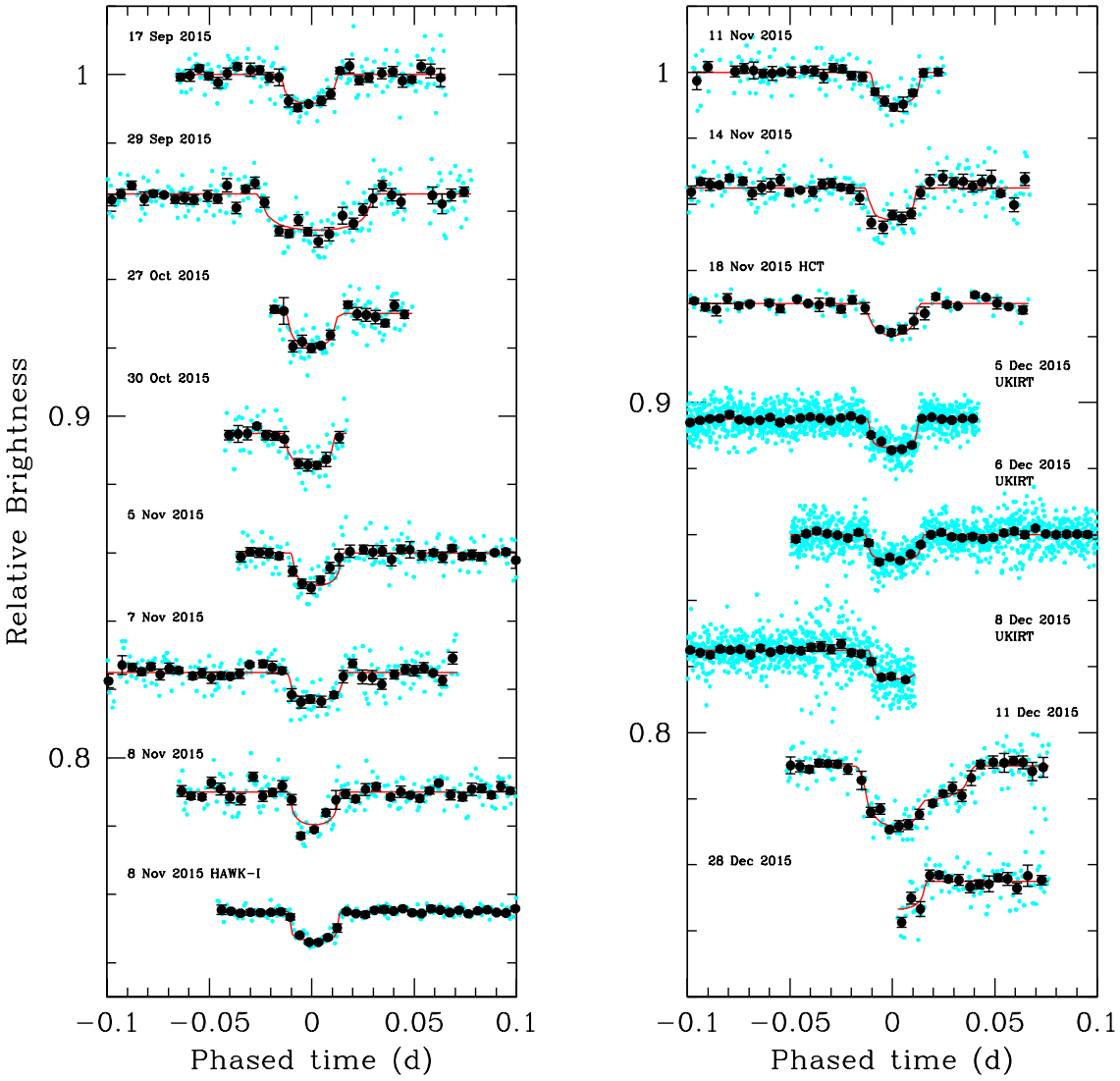

543

544 **Extended Data Figure 2 | Detrended TRAPPIST-1 transit light curves.** Same as Extended
545 Data Fig. 1, except that the light curves are here divided by the best-fit baseline model to
546 highlight the transit signatures.
547

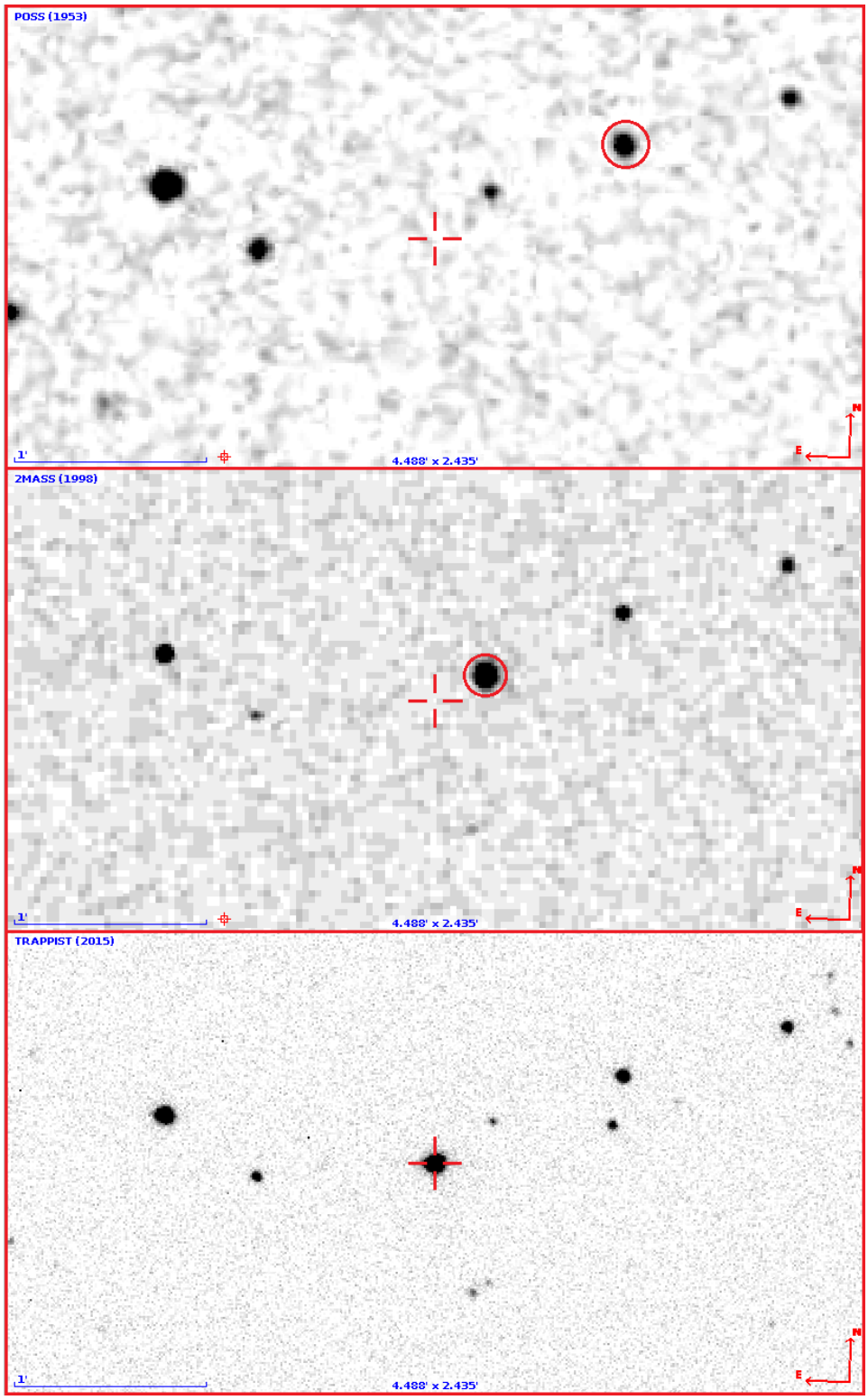

Extended Data Figure 3 | Position of TRAPPIST-1 in 1953, 1998, and 2015. The current position of the star as seen in the TRAPPIST images (bottom) is shown by a red cross in all panels, while its position in 1953 (POSS image, top) and 1998 (2MASS image, middle) is indicated by a red circle.

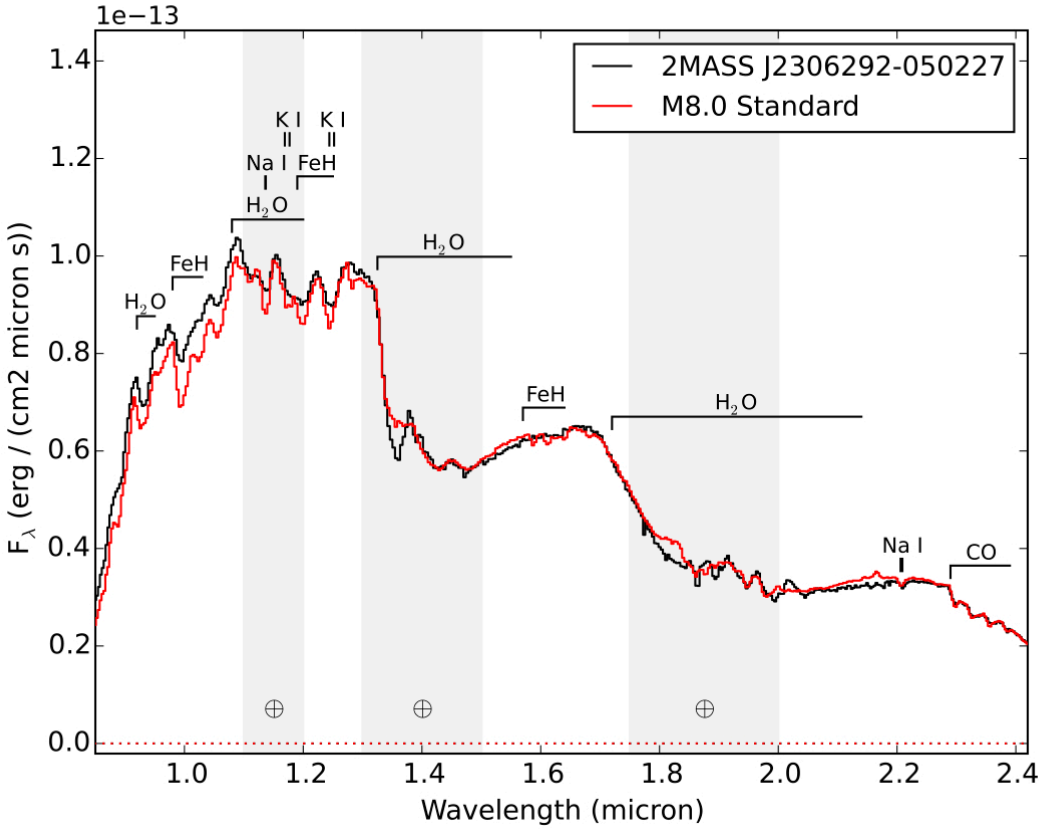

Extended Data Figure 4 | Near-infrared spectrum of TRAPPIST-1. Comparison of TRAPPIST-1's near-infrared spectrum obtained with the spectrograph IRTF/SpeX[35] and the spectrum of the M8-type standard LHS132 (red).

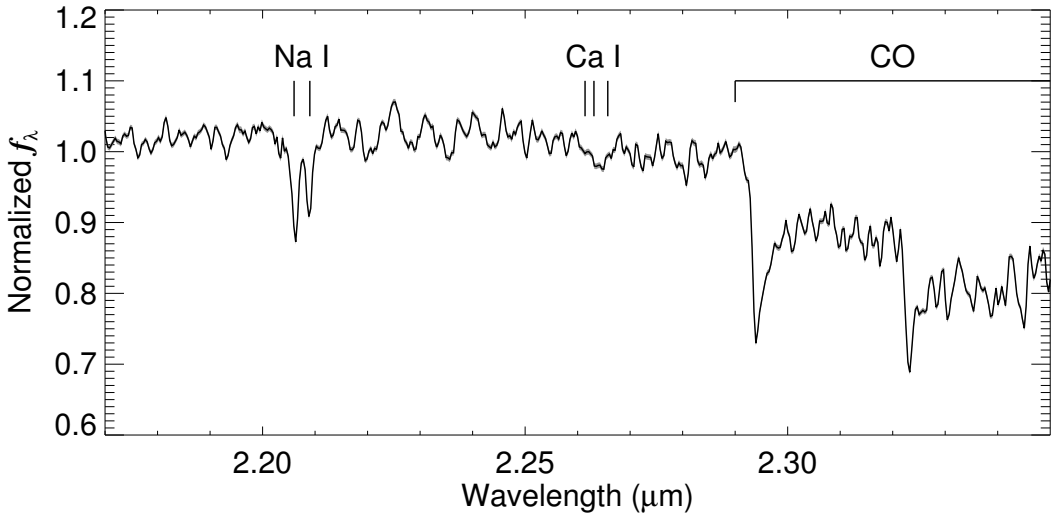

560

561 **Extended Data Figure 5 | SpeX cross-dispersed spectrum of TRAPPIST-1 in the 2.17-**
562 **2.35 μm region.** NaI, CaI and CO features are labelled. Additional structure is primarily from
563 overlapping H_2O bands. The spectrum is normalized at 2.2 μm.
564

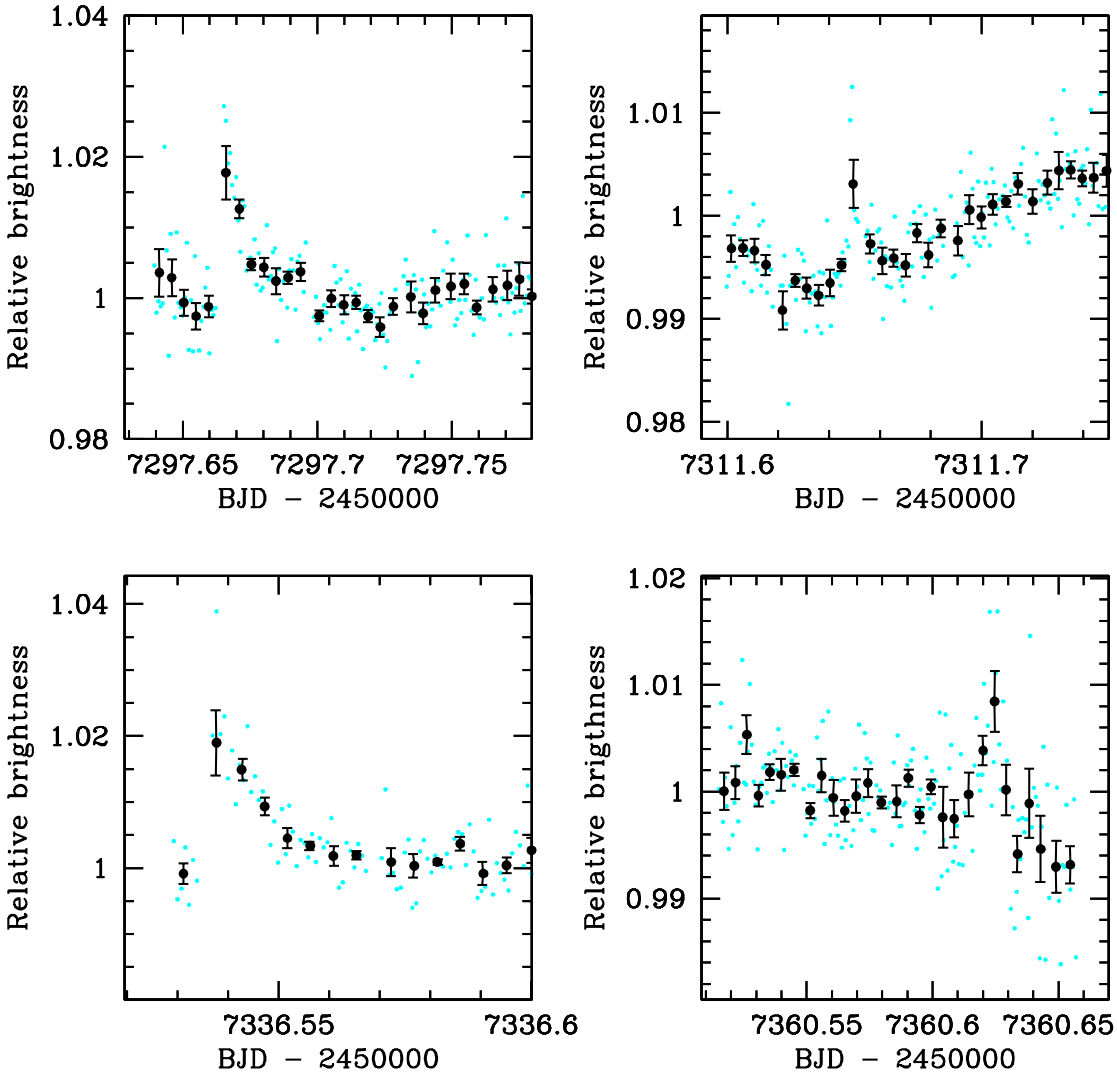

Extended Data Figure 6 | Flare events in the TRAPPIST 2015 photometry. The photometric measurements are shown unbinned (cyan dots) and binned per 7.2 minute intervals. For each interval, the error bars are the standard error of the mean.

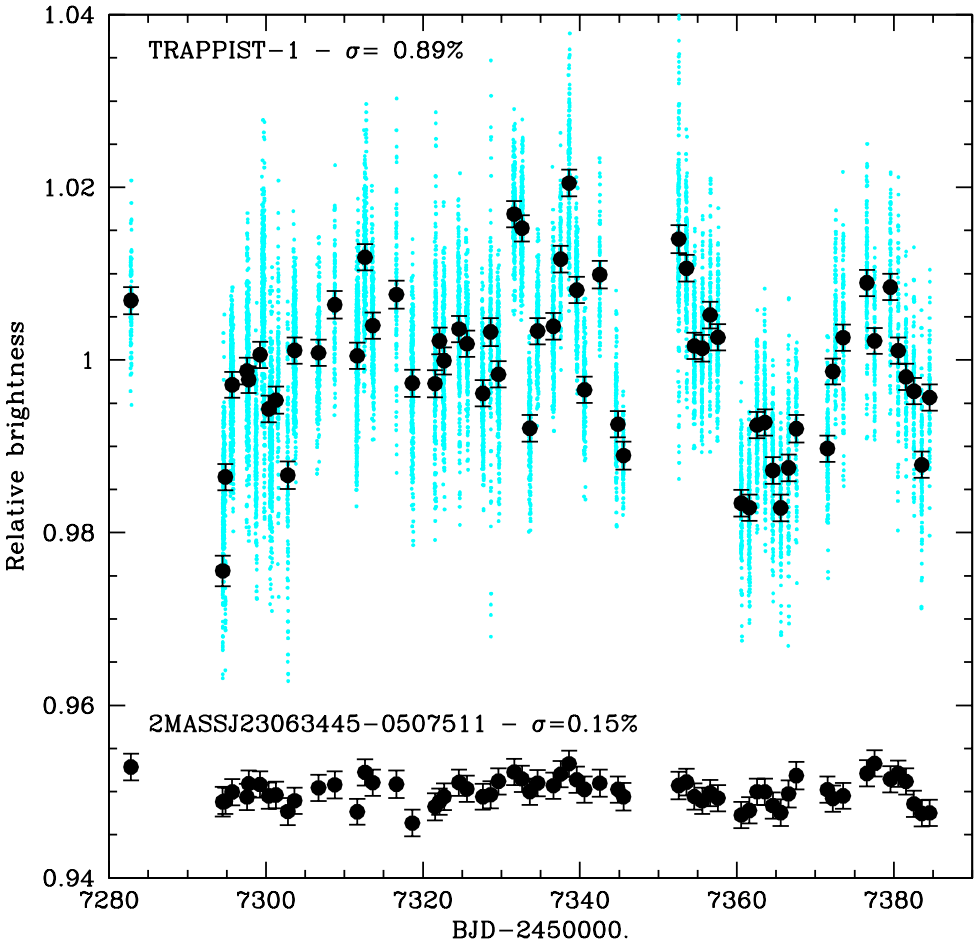

Extended Data Figure 7 | Variability light curve of TRAPPIST-1. The photometric measurements are shown unbinned (cyan dots) and binned per night (black dots with error bars = standard errors of the mean)**.** It is compared to the light curve of the comparison star 2MASSJ23063445-0507511, shifted along the y-axis for the sake of clarity.

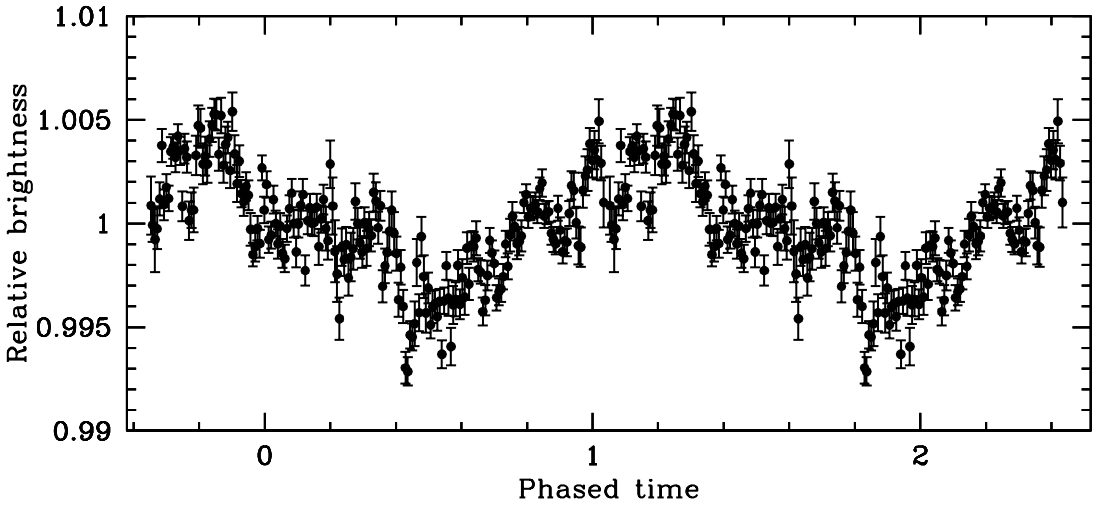

Extended Data Figure 8 | Time-phased variability light curve of TRAPPIST-1. The light curve is phased on the period P=1.40-days and binned per 10-min time intervals. The error bars are the standard errors of the mean of the measurements in the bins. Two periods are shown in the figure for the sake of clarity.

Extended Data Table 1. TRAPPIST-1 transit light curves.

Date	Instrument	Filter	N_p	T_{exp}	Baseline function	Transit(s)
17 Sep 2015	TRAPPIST	I+z	163	55s	$p(t^2+xy^2+f^2)$	TRAPPIST-1c
29 Sep 2015	TRAPPIST	I+z	232	55s	$p(t^2+xy^2+f^2)$	TRAPPIST-1d
27 Oct 2015	TRAPPIST	I+z	84	55s	$p(t^2+xy^2+f^2)$	TRAPPIST-1b
30 Oct 2015	TRAPPIST	I+z	77	55s	$p(t^2+xy^2+f^2)$	TRAPPIST-1b
05 Nov 2015	TRAPPIST	I+z	237	55s	$p(t^2+xy^2+f^2)$	TRAPPIST-1b
07 Nov 2015	TRAPPIST	I+z	241	55s	$p(t^2+xy^2+f^2)$	TRAPPIST-1c
08 Nov 2015	TRAPPIST	I+z	231	55s	$p(t^2+xy^2+f^2)$	TRAPPIST-1b
	VLT/HAWK-I	NB2090	207	17x1.7s	$p(t^2+xy^2+f^2)$	TRAPPIST-1b
11 Nov 2015	TRAPPIST	I+z	140	55s	$p(t^2+xy^2+f^2)$	TRAPPIST-1b
14 Nov 2015	TRAPPIST	I+z	241	55s	$p(t^2+xy^2+f^2)$	TRAPPIST-1b
18 Nov 2015	HCT/HFOSC	I	103	20s	$p(t^2+xy^2+f^2)$	TRAPPIST-1b
05 Dec 2015	UKIRT	J	1312	3x2s	$p(t^2+xy^2+f^2)$	TRAPPIST-1b
06 Dec 2015	UKIRT	J	1175	5x1s	$p(t^2+xy^2+f^2)$	TRAPPIST-1c
08 Dec 2015	UKIRT	J	1109	5x1s	$p(t^2+xy^2+f^2)$	TRAPPIST-1b
11 Dec 2015	TRAPPIST	I+z	158	55s	$p(t^2+xy^2+f^2)$	TRAPPIST-1c + d
28 Dec 2015	TRAPPIST	I+z	94	55s	$p(t^2+xy^2+f^2)$	TRAPPIST-1c (partial)

For each light curve, the instrument, filter, number of points N_p, exposure time T_{exp}, and baseline function are given. For the baseline functions, $p(\varrho^2)$ denotes, respectively, a 2^{nd}-order polynomial function of time (ϱ = t), x and y positions (ϱ = xy), and full-width at half-maximum of the stellar images (ϱ = f).

Extended Data Table 2 | Quadratic limb-darkening coefficients.

Bandpass	u_1	u_2
I (HCT/HFOSC)	0.72±0.10	0.15±0.11
I+z (TRAPPIST)	0.65±0.10	0.28±0.12
J (UKIRT/WFCAM)	0.10±0.05	0.57±0.02
NB2090 (VLT/HAWKI)	0.04±0.03	0.50±0.03

These values and errors for the quadratic coefficients u_1 and u_2 were inferred for TRAPPIST-1 from Claret & Bloemen (2011) tables[63], and used as a priori knowledge of the stellar limb-darkening in the global MCMC analysis of the transit light curves. The error bars were obtained by propagation of the errors on the stellar gravity, metallicity, and effective temperature.

Extended Data Table 3 | Posterior likelihoods of the orbital solutions for TRAPPIST-1d.

TRAPPIST-1d period (d)	**Circular orbit**	**Eccentric orbit**	***a*** **(au)**	S_p (S_{Earth})
4.551	0.0016	0.0017	0.023	0.98
5.200	0.0041	0.0045	0.025	0.82
8.090	0.012	0.013	0.034	0.45
9.101	0.018	0.011	0.037	0.39
10.401	0.139	0.0067	0.040	0.33
12.135	0.243	0.0029	0.045	0.26
14.561	0.393	0.0023	0.050	0.21
18.204	1	0.0018	0.058	0.15
24.270	0.212	0.0016	0.071	0.11
36.408	0.122	0.0014	0.093	0.06
72.820	$7.5e^{-5}$	$6.8e^{-8}$	0.147	0.02

The likelihoods shown are normalized to the most likely solution (circular orbit - P=18.204-d). For each orbit, the semi-major axis *a* is given in astronomical units (au), assuming a stellar mass of 0.08 $M_{\odot}$ (Table 1), and the mean irradiation, S_p, in Earth units, S_{Earth}.

Extended Data Table 4 | Individual timings measured for the TRAPPIST-1 planets.

Planet	Instrument	Epoch	Mid-transit timing (BJD_{TDB}-2,450,000)
TRAPPIST-1b	TRAPPIST	0	$7322.5161^{+0.0013}_{-0.0010}$
	TRAPPIST	2	$7325.5391^{+0.0035}_{-0.0013}$
	TRAPPIST	6	7331.5803±0.0013
	TRAPPIST	8	7334.6038±0.0012
	VLT/HAWK-I	8	7334.60490±0.00020
	TRAPPIST	10	7337.6249±0.0010
	TRAPPIST	12	$7340.6474^{+0.0010}_{-0.0022}$
	HCT/HFOSC	15	7345.18011±0.00089
	UKIRT/WFCAM	26	7361.79960±0.00030
	UKIRT/WFCAM	28	7364.82137±0.00056
TRAPPIST-1c	TRAPPIST	0	7282.8058±0.0010
	TRAPPIST	21	7333.6633±0.0010
	UKIRT/WFCAM	33	7362.72623±0.00040
	TRAPPIST	35	7367.5699±0.0012
	TRAPPIST	42	7384.5230±0.0011
TRAPPIST-1d	TRAPPIST	0	7294.7736±0.0014
	TRAPPIST	?	7367. 5818±0.0015

The transit timings shown were deduced from individual analyses of the transit light curves, assuming circular orbits for the planets. The error bars correspond to the 1-sigma limits of the posterior PDFs of the transit timings.

1. Kirkpatrick, J. D., Henry, T. J. & Simon, D. A. The solar neighborhood. 2: the first list of dwarfs with spectral types of M7 and cooler, *Astron. J.* **109**, 797 (1995).

2. Cantrell, J. R., Henry, T. J. & White, R. J. The solar neighborhood XXIX: the habitable real estate of our nearest stellar neighbours. *Astron. J.* **146**, 99 (2013)

3. Andrews, S. M., Wilner, D. J., Hugues, A. M., Qi, C. & Dullemond, C. P. Protoplanetary disk structures in Opiuchus. II. Extension to fainter sources. *Astrophys. J.* **723**, 1241 (2010).

4. Lyu, Y., Joergens, V., Bayo, A., Nielbock, M. & Wang, H. A homogeneous analysis of disk around brown dwarfs. *Astron. & Astrophys.* **582**, 22 (2015)

5. Payne, M. J. & Lodato, G. The potential for Earth-mass planet formation around brown dwarfs. *Mon. Not. R. Astron. Soc.* **381**, 1597 (2007)

6. Raymond, S. N., Scalo, J. & Meadows, V. S. A decreased probability of habitable planets formation around low-mass stars. *Astrophys. J.* **669**, 606 (2007).

7. Montgomery, R. & Laughlin, G. Formation and detection of Earth-mass planets around low mass stars. *Icar.* **202**, 1 (2009)

8. Kopparapu, R. K. *et al.* Habitable zones around main-sequence stars: new estimates. *Astrophys. J.* **765**, 131 (2013).

9. Gillon, M. *et al.* TRAPPIST: a robotic telescope dedicated to the study of planetary systems. *EPJ Web Conf.* **11**, 06002 (2011).

10. Gillon, M., Jehin, E., Fumel, A., Magain, P. & Queloz, D. TRAPPIST-UCDTS: a prototype search for habitable planets transiting ultra-cool stars. *EPJ Web Conf.* **47**, 03001 (2013). at <http://www.epj-conferences.org/articles/epjconf/abs/2013/08/epjconf_hpcs2012_03001/epjconf_hpcs2012_03001.html>

11. Gillon, M. *et al.* Fast-evolving weather for the coolest of our two new substellar neighbours. *Astron. & Astrophys.* **555**, L5 (2013)

12. Gillon, M. *et al.* SPECULOOS: Search for habitable Planets EClipsing ULtra-cOOl Stars. *Protostars and Planets VI*, poster #2K066 (2013). at <http://www.mpia.de/homes/ppvi/posters/2K066.pdf>

13. Liebert, J. & Gizis, J. E. RI photometry of 2MASS-selected late M and L dwarfs. *Publ. Astron. Soc. Pac.* **118**, 843 (2006).

14. Costa, E. *et al.* The solar neighbourhood. XVI. Parallaxes from CTIOPI: final results from the 1.5m telescope program. *Astron. J.* **132**, 1234 (2006).

15. Filippazzo, J. C. *et al.* Fundamental parameters and spectral energy distributions of young and field age objects with masses spanning the stellar to planetary regime. *Astrophys. J.* **810**, 158 (2015).

16. Gillon, M., *et al.* The TRAPPIST survey of southern transiting planets. I. Thirty eclipses of the ultra-short period planet WASP-43 b. *Astron.& Astrophys.,* **524**, 4 (2012).

17. Reiners, A. & Basri G. A volume-limited sample of 63 M7-M9.5 dwarfs. II. Activity, magnetism, and the fade of the rotation-dominated dynamo. *Astrophys. J.* **710**, 924 (2010).

18. Hosey, A. D. *et al*. The solar neighbourhood. XXXVI. The long-term photometric variability of nearby red dwarfs in the VRI optical bands, *Astron. J.* **150**, 6 (2015).

19. Liang, Y. *et al.* Tests of the planetary hypothesis for PTFO8-8695b. *Astrophys. J.* **812**, 48 (2015).

20. Stelzer, B. Marino, A., Micela, G., López-Santiago, J. & Liefke, C. The UV and X-ray activity of the M dwarfs within 10 pc of the Sun. *Mon. Not. R. Astron. Soc.* **431**, 2063 (2013).

21. Lopez, E. D., Fortney, J. J. & Miller, N. How thermal evolution and mass-loss sculpt populations of super-Earths and sub-Neptunes: Application to the Kepler-11 system and beyond. *Astrophys. J.,* **761**, 59 (2012).

22. Seager, S., Kuchner, M., Hier-Majumder, C. A. & Militzer, B. Mass-radius relationships for solid exoplanets. *Astrophys. J.,* **669**, 1279 (2007).

23. Artigau, E. *et al.* SPIRou: the near-infrared spectropolarimeter/high-precision velocimeter for the Canada-France-Hawaii telescope. *Proc. SPIE* **9147**, 15A (2014). doi:10.1117/12.2055663

24. Holman, M. J. & Murray, N. W. The use of transit timing to detect terrestrial-mass extrasolar planets. *Science* **307**, 1288 (2005).

25. Kasting, J. F., Whitmire, D. P. & Reynolds, R. T. Habitable zones around main-sequence stars. *Icar.* **101**, 108 (1993).

26. Leconte, J. *et al.* 3D climate modelling of close-in land planets: Circulation patterns, climate moist instability, and habitability. *Astron. & Astrophys.* **554**, 69 (2013).

27. Menou, K. Water-trapped world. *Astrophys. J.,* **774**, 51 (2013).

28. Driscoll, P. E. & Barnes, R. Tidal heating of Earth-like exoplanets around M stars: thermal, magnetic, and orbital evolutions. *Astrobio*. **15**, 739 (2015).

29. De Wit, J. & Seager, S. Constraining exoplanet mass from transmission spectroscopy. *Science* **342**, 1473 (2013).

30. Snellen, I. A. G., de Kock, R. J., de Mooij, E. J. W. & Albrecht, S. The orbital motion, absolute mass and high-altitude winds of exoplanet HD209458b. *Nature* **465**, 1049 (2010).

31. Gizis, J. E. *et al.* New neighbours from 2MASS: activity and kinematics at the bottom of the main sequence. *Astron. J.* **120**, 1085 (2000).

32. Bartlett, J. L. Knowing our neighbours: Fundamental properties of nearby stars. *Publ. Astron. Soc. Pac*. **119**, 857 (2007).

33. Schmidt S. J., Cruz, K. L., Bongiorno, B. J., Liebert, J. & Reid, I. N. Activity and kinematics of ultracool dwarfs, including an amazing flare observation. *Astron. J.* **133**, 2258 (2007).

671 34. Lee, K.-G., Berger, E. & Knapp, G. R. Short-term Hα variability in M dwarfs. *Astrophys. J.* **708**, 1482
672 (2010).

673 35. Rayner, J. T. *et al.* SpeX: A Medium-Resolution 0.8-5.5 Micron Spectrograph and Imager for the
674 NASA Infrared Telesce. *Publ. Astron. Soc. Pac*. **115**, 362 (2003).

675 36. Reiners, A. & Basri G. A volume-limited sample of 63 M7-M9.5 dwarfs. I. Space motion, kinematics
676 age, and lithium. *Astrophys. J.* **705**, 1416 (2009).

677 37. Vacca, W. D., Cushing, M. C. & Rayner, J. T. A Method of Correcting Near-Infrared Spectra for
678 Telluric Absorption. *Publ. Astron. Soc. Pac*. **115**, 389 (2003).

679 38. Cushing, M. C.,Vacca, W. D. & Rayner, J. T. Spextool: a spectral extraction package for SpeX, a 0.8-
680 5.5 micron cross-dispersed spectrograph. *Publ. Astron. Soc. Pac*. **116**, 362 (2004).

681 39. Rojas-Ayala, B., Covey, K. R., Muirhead, P. S. & Lloyd, J. P. Metallicity and temperature indicators in
682 M dwarf K-band spectra: testing new and updated calibrations with observations of 133 solar neighbourhood M
683 dwarfs. *Astrophys. J.* **748**, 93 (2012).

684 40. Mann, A. W. *et al.* Prospecting in ultracool dwarfs: measuring the metallicities of mid- and late-M
685 dwarfs. *Astron. J.* **147**, 160 (2014).

686 41. Skrutskie, M. F., Meyer, M. R., Whalen, D. & Hamilton, C. The two micron all sky survey (2MASS).
687 *Astron. J.* **131**, 1163 (1996).

688 42. Cutri, R. M. *et al.* Vizier Online Data Catalog II/311: WISE all-sky data release (2012). at
689 <http://vizier.cfa.harvard.edu/viz-bin/VizieR?-source=II/311>

690 43. Cruz, K. L. et al. Meeting the cool neighbours. IX. The luminosity function of M7-L8 ultracool dwarfs
691 in the field. *Astron. J.* **133**, 439 (2007).

692 44. Baraffe, I., Homeier, D., Allard, F. & Chabrier, G. New evolutionary models for pre-main sequence
693 and main sequence low-mass stars down to the hydrogen-burning limit. *Astron. & Astrophys.* **577**, 42 (2015).

694 45. Siegler, N., Close, L. M., Mamajeck, E. E. & Freed, M. An adaptive optics survey of M6.0-M7.5 stars:
695 discovery of three very low mass binary system including two probable Hyades member. *Astrophys. J.* **598**,
696 1265 (2003).

697 46. Siegler, N., Close, L. M., Cruz, K. L., Martín, E. L. & Reid, I. N. Discovery of two very low mass
698 binaries: final results of an adaptive optics survey of nearby M6.0-M7.5 stars. *Astrophys. J.* **621**, 1023 (2005).

699 47. Janson, M. *et al.* The AstraLux large M-dwarf multiplicity survey. *Astrophys. J.* **754**, 44 (2012).

700 48. Bouy H. *et al.* Multiplicity of nearby free-floating ultracool dwarfs: a Hubble Space Telescope WFPC2
701 search for companions. *Astron. J.* **126**, 1526 (2003).

702 49. Barnes, J. R. *et al.* Precision radial velocities of 15 M5-M9 dwarfs. *Mon. Not. R. Astron. Soc.* **439**,
703 3094 (2014)

704 50. Tanner, A. *et al.* Keck NIRSPEC radial velocity observations of late M-dwarfs. *Astrophys. J.* **203**
705 (Suppl.), 10 (2012).

706 51. Burgasser, A. J. *et al.* WISE J072003.20-084651.2: and old and active M9.5 + 75 spectral binary 6 pc
707 from the Sun. *Astron. J.* **149**, 104 (2015).

708 52. Zacharias, N. *et al.* The second US Naval Observatory CCD astrograph catalog (UCAC2). *Astron. J.*
709 **127**, 3043 (2004).

710 53. Izmailov, I. S. *et al.* Astrometric CCD observations of visual double stars at the Pulkovo Observatory.
711 *Astron. L.* **36**, 349 (2010).

712 54. Minkowski, R. L. & Abell, G. O. The National Geographic Society-Palomar Observatory Sky Survey.
713 *Basic Astronomical Data: Stars and stellar systems*, edited by K. A. Strand, University of Chicago Press,
714 Chicago, IL USA, 481 (1963).

715 55. Jehin, E., *et al.* TRAPPIST: TRAnsiting Planets and PlanetesImals Small Telescope. *Msngr* **145**, 2
716 (2011). at <https://www.eso.org/sci/publications/messenger/archive/no.145-sep11/messenger-no145-2-6.pdf>

717 56. Stetson, P. B. DAOPHOT - A computer program for crowded-field stellar photometry. *Publ. Astro.*
718 *Soc. Pacific*, **99**, 191 (1987).

719 57. at <http://www.iiap.res.in/iao_hfosc>

720 58. Pirard, J.-F. *et al.* HAWK-I: A new wide-field 1- to 2.5 μm imager for the VLT. *Proc. SPIE* **5492**,
721 1763 (2004). doi:10.1117/12.578293

722 59. Casali, M. *et al.* The UKIRT IR Wide-Field Camera (WFCAM). In *The new era of of wide-field*
723 *astronomy*, *ASPC Conference Series Vol. 232* (eds Clowes, R., Adamson, A. & Bromage, G.) 357 (2001).

724 60. Eastman, J., Siverd, R. & Gaudi, B. S. Achieving Better Than 1 Minute Accuracy in the Heliocentric
725 and Barycentric Julian Dates. *Publ. Astro. Soc. Pacific*, **122**, 935 (2010).

726 61. Mandel, K. & Agol, E. Analytic light curves for planetary transit searches. *Astrophys. J.* **580**, 181
727 (2002).

728 62. Schwarz, G. Estimating the dimension of a model. *Ann. Statist.* **6**, 461 (1978).

729 63. Claret, A. & Bloemen, S. Gravity and limb-darkening coefficients for the Kepler, CoRoT, Spitzer,
730 uvby, UBVRIJHK, and Sloan photometric systems. *Astron. & Astrophys.* **529**, 75 (2011).

731 64. Gelman, A. & Rubin. , D. B. Inference from Iterative Simulation Using Multiple Sequences. *Statist.*
732 *Sciences* **7**, 457 (1992).

733 65. Winn, J. N. Exoplanets transits and occultations. *Exoplanets,* eds. S. Seager, University of Arizona
734 Press (2010).

735 66. Agol, E., Steffen, J., Sari, R. & Clarkson, W. On detecting terrestrial planets with timing of giant planet
736 transits. *Mon. Not. R. Astron. Soc.* **359**, 567 (2005).

67. Davenport, J. R. A. *et al.* Kepler flares II: the temporal morphology of white-light flares on GJ1243. *Astrophys. J.* **797**, 122 (2014).

68. Scargle, J. D. Studies in astronomical time series analysis. II - Statistical aspects of spectral analysis of unevenly spaced data. *Astrophys. J.* **263**, 835 (1982).

69. Goldreich, P. & Soter, S. Q in the solar system. *Icarus* **5**, 375 (1966).

70. Murray, C. D. & Dermott, S. F. *Solar system Dynamics*, Cambridge University Press (2001).

71. Limbach, M. A. & Turner, E. L. The orbital eccentricity - multiplicity relation and the solar system. *Proc. Nat. Ac. Sci.* **112**, 20 (2015).

72. Chambers, J. E. & Migliorini F. Mercury: a new software package for orbital integrations. *DPS meeting* 29, 1024 (1997). at <http://adsabs.harvard.edu/abs/1997DPS....29.2706C>

73. Charbonneau, D. *et al.* A super-Earth transiting a nearby low-mass star. *Nature* **462**, 891 (2009).

74. Miller-Rici, E., Seager, S. & Sasselov, D. The atmospheric signatures of super-Earths: how to distinguish between hydrogen-rich and hydrogen-poor atmospheres. *Astrophys. J.* **690**, 1056 (2009).

75. Han, E. *et al.* The exoplanet orbit database. II. Updates to exoplanet.org. *Publ. Astro. Soc. Pacific*, **126**, 827 (2014).

76. Kreidberg, L. *et al.* Clouds in the atmosphere of the super-Earth exoplanet GJ1214b. *Nature* **505**, 69 (2014).

77. Berta, Z. K. *et al.* The flat transmission spectrum of the super-Earth GJ1214b from Wide Field Camera 3 on the Hubble Space Telescope. *Astrophys. J.,* **747**, 35 (2012).

78. Rodler, F. & López-Morales, M. Feasibility studies for the detection of O_2 in an Earth-like exoplanet. *Astrophys. J.,* **781**, 54 (2014).

79. Bonnarel, F. *et al.* The ALADIN interactive sky atlas. A reference tool for identification of astronomical sources. *Astron. & Astrophys. Sup.* **143**, 33 (2000).

SUPPLEMENTARY METHODS

Estimation of the suitability of the planets for detailed atmospheric characterization. We estimated the typical signal amplitude in transit transmission spectroscopy for all the transiting exoplanets with a size equal to or smaller than the mini-Neptune GJ1214b[73]. We computed it as $2R_p h_{eff}/R_*^2$ where R_p is the planetary radius, h_{eff} the effective atmospheric height (i.e., the extent of the atmospheric annulus), and R_* is the stellar radius. The effective atmospheric height is directly proportional to the atmospheric scale height, $H=kT/(\mu g)$ where k is Boltzmann's constant, T the atmospheric temperature, μ the atmospheric mean molecular mass, and g the surface gravity. The ratio h_{eff}/H for a clear atmosphere[29, 74] is typically between 6 and 10 and is thus strongly dependent on the presence of clouds and the spectral resolution and range covered. Our estimates, presented in Fig. 3, are based on an h_{eff}/H ratio of 7 and the conservative assumption of a volatile-dominated atmosphere (μ=20) with a Bond albedo of 0.3. All other parameters for the planets were derived from exoplanets.org[75]. As illustration, the maximum transit depth variations projected under those assumptions for GJ1214b are of ~250 ppm, in agreement with independent simulations[76].

We also derived for the same planets sample typical SNRs in transit transmission spectroscopy from the ratio of our computed signal amplitudes over the square root of the flux (determined from the J-band magnitudes of the host stars). The SNRs of TRAPPIST-1's planets in transmission are expected to range between 0.35 and 0.55 times GJ 1214b's, implying that TRAPPIST-1's planets are well-suited for atmospheric studies with HST/WFC3 similar to those previously targeting GJ1214b[76, 77].

Based on the simulations for terrestrial planets performed by de Wit & Seager[29] and following their Equations S.34 and S.35, we estimated that the characterization of TRAPPIST-1 b, TRAPPIST-1 c, and TRAPPIST-1 d should require up to 70, 90, and 150 hrs of in-transit observations with JWST, respectively, and yield the planet masses, atmospheric temperatures, and abundances with a relative uncertainty below 20%, 15%, and 300% (i.e., within a factor of 4), respectively. Assuming the atmospheres of TRAPPIST-1's planets are not depleted and do not harbor a high-altitude cloud deck, JWST should notably yield constraints on the abundances of molecules with large absorption bands such as H_2O, CO_2, CH_4, CO, and O_3 if their abundances are ≥10-ppm level.

To assess the potential of the cross-correlation technique[30] to constrain the atmospheric properties of the TRAPPIST-1 planets, we followed Rodler and Lopez-Morales (2013)[78]. We inferred that detecting O_2 in TRAPPIST-1's planets would require up to 80 transit observations with one of the next generation giant ground-based telescopes. Taking in account the limited fraction of transits visible at low airmass, such an endeavor could be reached in 5 to 15 years.

SUPPLEMENTARY NOTES

Timeline of the observations.

A planetary transit signature was discovered in the TRAPPIST 1 light curve observations taken on 17 September 2015. It triggered an intense monitoring of the star with the TRAPPIST telescope. In the first phase, additional transit signatures were detected during the nights of 29 September, 27 and 30 October 2015. The analysis of the corresponding light curves with our adaptive MCMC code (see Methods) led to the conclusion that the first three transit signatures exhibited significantly different parameters (depths and/or durations) and that, provided these were of planetary origin, they must originate from three different planets (TRAPPIST 1b, 1c, and 1d). This analysis also resulted in parameters for the transits of 27 and 30 October 2015 that were consistent with one another, suggesting they originated from the same planet. Based on these results, a third transit of similar shape was predicted for 5 November 2015, and was subsequently confirmed. With a well-constrained transit ephemeris for one of the planets, we triggered follow-up observations with the ESO VLT/HAWK-I to confirm the orbital period and to obtain a high-precision near-IR light curve to assess its achromaticity and to precisely measure the transit shape parameters. These HAWK-I observations, performed during the night of 8 November 2015, resulted in a light curve displaying a clear transit-signal at the expected time. Analyzing this with the MCMC code resulted in transit parameters in excellent agreement with those derived for the TRAPPIST transits, confirming it originated from a planet whose size is Earth-like, TRAPPIST-1b. The TRAPPIST telescope observed other transits of TRAPPIST-1b on 8 November (concurrently with VLT/HAWK-I), 11 and 14 November 2015.

At that stage, two orbital periods were possible for the TRAPPIST-1b planet based on the TRAPPIST+HAWK-I dataset, 3.02 days and 1.51 days, the shorter period being only mildly favored by an MCMC analysis, assuming a circular orbit for the planet and the *a priori* knowledge of the stellar properties. Because its value is nearly resonant with the Earth's rotational period, confirming this period of 1.51 days required requesting observations of the star from a site with a longitude offset of ~180° compared to Chile. We thus obtained observations from India with the HCT/HFOCS instrument corresponding to a period of 1.51 days. The observations, performed on 18 November 2015, resulted in a differential light curve that demonstrated a clear transit at the predicted time, confirming the period of 1.51 days for TRAPPIST-1b.

On 7 November 2015, the TRAPPIST telescope recorded a transit-signal that was consistent with the very first transit-signal observed on 17 September 2015. Assuming that these two similar transits originated from the same transiting planet, our TRAPPIST dataset allowed us to constrain its orbital periods to several values. Because of the rarity of the possible transit events visible by TRAPPIST before the end of the visibility season of the star, we triggered observations of a possible transit window of this planet candidate, and of two transits of TRAPPIST-1b, on UKIRT/WFCAM (Hawaii). The UKIRT observations were performed on 5, 6 and 8 December 2015. The light curves from 5 and 8 December showed the predicted transits of TRAPPIST-1b, while the light curve of 6 December exhibited a brightness drop similar in amplitude and duration to the transit-signals observed on 17 September and 7 November, at a time fully consistent with three of the periods derived from these two

847 previous signals, namely P=2.422 days, 3.633 days, and 7.265 days. On 11 December 2015,
848 TRAPPIST recorded another eclipse at the time corresponding to the period of P=2.422 days.
849 Still, this eclipse was anomalous (too long, too deep, and highly asymmetric). Further
850 analysis revealed that it is well represented by a dual transit of TRAPPIST-1c, confirming for
851 1c the period P=2.422 days, and of the object that transited in front of the star on 29
852 September 2015. We thus attributed the second transit in the 11 December light curve to a
853 third planet, TRAPPIST-1d, for which two transits were observed by TRAPPIST (29
854 September and 11 December). Finally, a partial transit of TRAPPIST-1c was observed by
855 TRAPPIST on 28 December 2015, at the time expected for its inferred period P=2.422 days.
856
857 **Acknowledgments**
858 The authors recognize and acknowledge the very significant cultural role and reverence that
859 the summit of Mauna Kea has always had within the indigenous Hawaiian community. We
860 are most fortunate and grateful to have the opportunity to conduct observations from this
861 mountain. The authors are very grateful to the Geneva Observatory, and especially to V.
862 Mégevand, and to the ESO La Silla staff, for their technical support for the operations of
863 TRAPPIST. We gratefully acknowledge ESO for its continuous supports to our projects
864 TRAPPIST and SPECULOOS. This research made us of Aladin[79].
865

SUPPLEMENTARY FIGURES

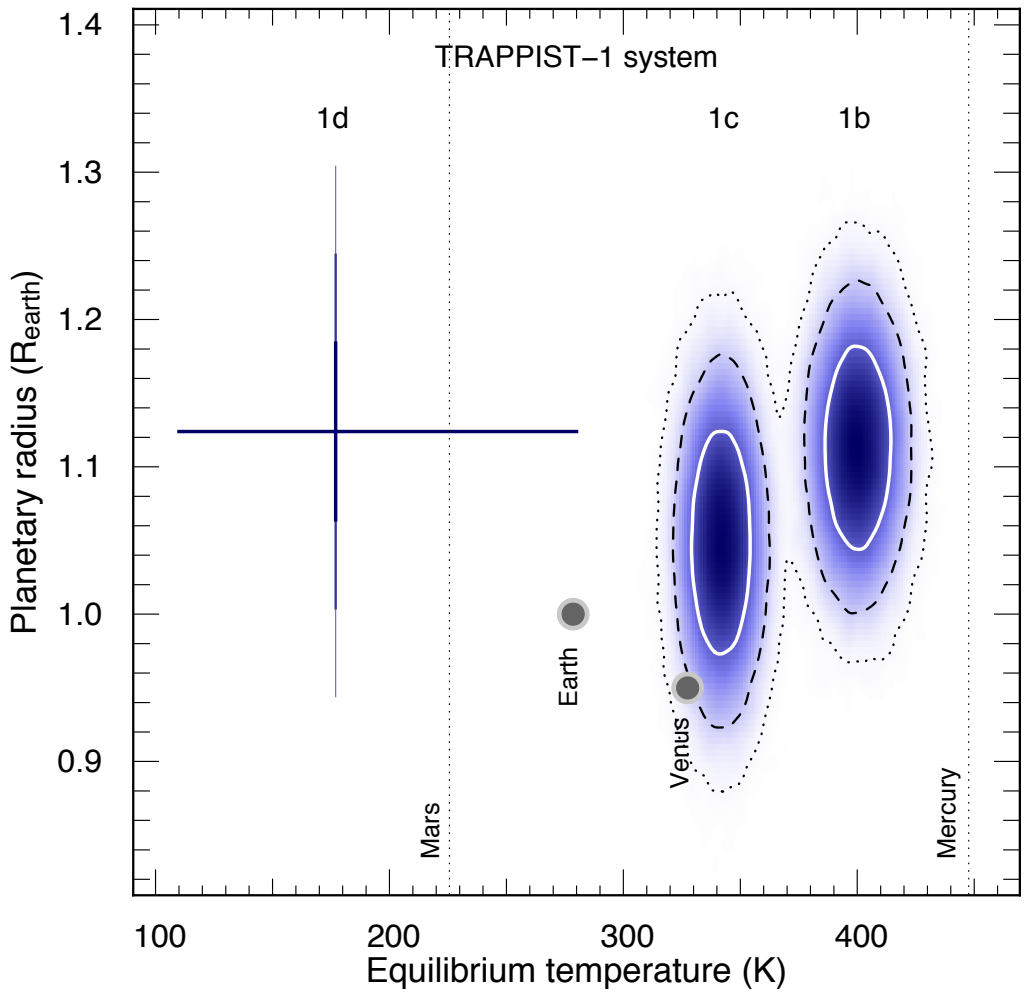

Supplementary Figure 1. Comparison of the TRAPPIST-1 planets in terms of temperature and size with the Solar system's terrestrial planets. The positions of Earth & Venus are represented with grey symbols while Mercury and Mars are shown with dotted lines. The two blue areas (1b & 1c) show the distribution of possible parameters for TRAPPIST-1b and TRAPPIST-1c, respectively. The white contour is the 1-sigma confidence region, while the black dashed and dotted lines represented the 2 and 3-sigma regions, respectively. TRAPPIST-1d is displayed differently to highlight the fact that its period (and consequently, its equilibrium temperature) remain uncertain, while its radius is well measured (its 1, 2, and 3-sigma error bars are shown). Equilibrium temperatures were computed assuming an albedo of 0 and neglecting atmospheric effects.